Oxygen diffusion impedance in proton exchange membrane fuel cells – insights into electrochemical impedance spectra and equivalent electrical circuit modeling

William Aït-Idir, Peizhe Wu, Ricardo Sgarbi, Quentin Labarde, Salah Touhami, Meriem Daoudi, Assma El Kaddouri, Jean-Christophe Perrin, Jérôme Dillet, Clémence Marty, et al.

Oxygen Diffusion Impedance in Proton Exchange Membrane Fuel Cells – insights into Electrochemical Impedance Spectra and Equivalent Electrical Circuit Modeling

William Aït-Idir , Peizhe Wu , Ricardo Sgarbi , Quentin Labarde , Salah Touhami , Meriem Daoudi , Assma El kaddouri , Jean-Christophe Perrin , Jérôme Dillet , Clémence Marty , Fabrice Micoud , Marian Chatenet , Olivier Lottin , Julia Mainka

PII: S0013-4686(23)01602-X
DOI: https://doi.org/10.1016/j.electacta.2023.143430
Reference: EA 143430

To appear in: *Electrochimica Acta*

Received date: 6 October 2023
Revised date: 30 October 2023
Accepted date: 30 October 2023

Please cite this article as: William Aït-Idir , Peizhe Wu , Ricardo Sgarbi , Quentin Labarde , Salah Touhami , Meriem Daoudi , Assma El kaddouri , Jean-Christophe Perrin , Jérôme Dillet , Clémence Marty , Fabrice Micoud , Marian Chatenet , Olivier Lottin , Julia Mainka , Oxygen Diffusion Impedance in Proton Exchange Membrane Fuel Cells – insights into Electrochemical Impedance Spectra and Equivalent Electrical Circuit Modeling, *Electrochimica Acta* (2023), doi: https://doi.org/10.1016/j.electacta.2023.143430

Highlights:

- Gas diffusion layer main contributor to low frequency diffusion impedance.
- High frequency resistance linked to O_2 diffusion through cathode ionomer.
- Most adapted circuit: Kulikovsky diffusion impedance in series with ORR kinetics.
- Local air inlet impedance spectrum less impacted by O_2 concentration oscillations.

Oxygen Diffusion Impedance in Proton Exchange Membrane Fuel Cells – insights into Electrochemical Impedance Spectra and Equivalent Electrical Circuit Modeling

William Aït-Idir[1**], Peizhe Wu[1**], Ricardo Sgarbi[2], Quentin Labarde[2], Salah Touhami[1], Meriem Daoudi[1], Assma El kaddouri[1], Jean-Christophe Perrin[1], Jérôme Dillet[1], Clémence Marty[3], Fabrice Micoud[3], Marian Chatenet[2], Olivier Lottin[1], Julia Mainka[1*]

[1]*LEMTA, CNRS, Université de Lorraine, Nancy, France*

[2]*Univ. Grenoble Alpes, Univ. Savoie Mont Blanc, CNRS, Grenoble INP (Institute of Engineering and Management Univ. Grenoble Alpes), LEPMI, 38000 Grenoble, France*

[3]*Univ. Grenoble Alpes, CEA, LITEN, F-38054, Grenoble, France*

**Corresponding author. E-mail address: Julia.mainka@univ-lorraine.fr*, Phone number: +33 (0)3 72 74 43 20, LEMTA - Université de Lorraine - UMR CNRS 7563, 2 avenue de la Forêt de Haye BP 90161, F-54505 Vandœuvre les Nancy Cedex

** The authors equally contributed to the work.

Keywords: Proton Exchange Membrane Fuel Cell, Electrochemical Impedance Spectroscopy, Oxygen Diffusion Impedance, Electrical Equivalent Circuit Modeling.

Nomenclature

ACL: Anode Catalyst Layer

CCL: Cathode Catalyst Layer

CCM: Catalyst Coated Membrane

CL: Catalyst Layer

DRT: Distribution of Relaxation Times

EDL: Electrical Double-Layer

EEC: Equivalent Electrical Circuit

EI: Electrochemical Impedance

EIS: Electrochemical Impedance Spectroscopy

FC: Fuel Cell

GDE: Gas Diffusion Electrode

GDL: Gas Diffusion Layer

HOR: Hydrogen Oxidation Reaction

HF: High Frequency

LF: Low Frequency

MEA: Membrane Electrode Assembly

MPL: Micro Porous Layer

ORR: Oxygen Reduction Reaction

PEMFC: Proton Exchange Membrane Fuel Cell

PFSA: PerFluoroSulfonic Acid

PTFE: PolyTetraFluoroEthylene

RH: Relative Humidity

RHE: Reference Hydrogen Electrode

TLM: Transmission Line Model

Abstract

In Randles circuit, the oxygen diffusion impedance connects in series with the Oxygen Reduction Reaction charge-transfer resistance, implying that the Cathode Catalyst Layer (CCL) governs oxygen diffusion. The oxygen diffusion impedance can be connected in series with the ORR circuit, implying that Gas Diffusion Layer (GDL) rules oxygen diffusion. The common finite Warburg element and an alternative expression for diffusion through GDL derived by Kulikovsky were tested and compared. For this, experimental data obtained from measurements on various cells geometries, MEA types and operating conditions were used. All cases yield the same trend: the low frequency diffusion impedance in PEMFC mainly relates to the GDL, or both the GDL *and* the CCL, the latter to a significantly lower extent. EI spectra measured for different cathode Pt-loadings suggest that the ionomer film inside the CCL contributes rather to the high-frequency resistance, increasingly at lower catalyst loading. Hence, the physically most appropriate equivalent electrical circuit is a Kulikovsky diffusion impedance connected in series with the ORR kinetics circuit. Comparing global and local impedance spectra confirmed the significant contribution of perturbation-induced oxygen concentration oscillations to the low frequency loop in Nyquist plots: analyzing local impedance data measured near the oxygen inlet allows to minimize their impact.

1. Introduction

Electrochemical Impedance Spectroscopy (EIS) is an extensively used technique for analyzing the operation of Proton Exchange Membrane Fuel Cells (PEMFCs) [1,2], Proton Exchange Membrane Water Electrolyzers [3–5], supercapacitors [6–8], batteries [9–11] and other electrochemical systems [12]. It allows to characterize the impedance of the whole system or some of its components [13] in-operando and to discriminate between various contributions such as reaction kinetics (charge-transfer), mass-transport, as well as the inductance of connecting systems. In the case of PEMFCs, it can be used to assess for instance the impact of operating conditions such as relative humidity, pressure, temperature, current density or composition of active materials on the cell performance, or to monitor material degradations [14–17].

EIS is based on the interpretation of sinusoidal variations of the current and cell voltage at a given operating point. The amplitude of the perturbation signal should be kept low enough, so that the system response (in terms of voltage or current) can be considered as linear, but also high enough to enable good signal/noise ratio. The impedance is measured in the frequency domain allowing to use different ways to interpret data [18]. The most common ones consist in using physical models and Equivalent Electrical Circuits (EECs). Physical models are derived from a set of equations describing the phenomena governing the system operation. These equations must be chosen carefully and may be challenging to solve, so that physical models are generally limited to single components and/or simple systems [18,19]. For more complex cases, like for instance multicomponent systems with more than a single electrochemical reaction, it is more convenient to use equivalent electrical circuits, i.e. the connection of several simple electrical elements. This makes it possible to reproduce the experimental impedance spectra, but attention must be paid to the physical meaning of each element. There are also other ways to interpret the impedance data, like the Distribution of Relaxation Times (DRT), which gained interest in the scientific community in the recent years [20–22]. This method is based on the analysis of the relaxation of an electrochemical system following the application of small current or voltage perturbations. The DRT spectrum is calculated from the standard impedance, and the exponential decay of the response is interpreted in terms of timescale distribution of the individual physical processes [18,21,23].

The Randles circuit is the most common EEC describing PEMFC single cells [24]. It is an electric equivalent representation of ion conduction through the membrane and reaction kinetics of the Oxygen Reduction Reaction (ORR, the limiting reaction in a PEMFC) as well as oxygen diffusion in the Cathode Catalyst Layer (CCL), the Anode Catalyst Layer (ACL) being generally negligible. Although extensively used, this circuit presents inherent physical limits. For instance, for a FC fed with air, some authors showed that oxygen diffusion limitations are mainly located in the GDL [25]. Other works point out that it might be rather the ionomer inside in the CCL which is limiting for oxygen transport. More specifically, the

impact of this layer seems to increase for low catalyst loaded electrodes and/or at low relative-humidity of the feeding gases, because of high local mass fluxes [26–28]. Finally, others put forward oxygen diffusion limitations in the pores of the CCL [29] which would agree with the Randles circuit. It seems that this contribution is however less important than that of the GDL [25]. On top of that, it has to be reminded that the impedance data are also impacted by oxygen concentration oscillations induced by the measuring signal perturbation [30–32] and by water fluxes [33]. Such phenomena are the most significant at low frequencies which is the range of the oxygen diffusion impedance.

In the Randles circuit, diffusion limitations are considered through a finite Warburg impedance Z_W [34] connected in series with the charge transfer resistance R_{ct} of the ORR [24]. This implies that oxygen diffusion is limited by the CCL (pores or ionomer). For diffusion through the GDL, Kulikovsky showed that the associated impedance expression should differ from the finite-length Warburg element, because mass transport is affected by the double-layer capacity C_{dl} of the porous catalyst layer (CL) [35]. He derived an alternative impedance expression for oxygen diffusion through the GDL which tends to Z_W when the double-layer capacity tends to zero. This extreme case corresponds to a thin (interfacial) electrode, which is exactly the hypothesis that underlies the derivation of the Warburg impedance. However, it must be pointed out that the thin interface hypothesis governing the derivation of Warburg impedance is in contradiction with the Randles circuit: indeed, Z_W and R_{ct} (connected in series) are in parallel with C_{dl} (Figure 2a). If the catalyst layer is assumed to be an interface, Z_W should rather be connected in series with the ORR kinetics circuit, i.e. the parallel connection of R_{ct} and C_{dl} (Figure 2b).

Oxygen diffusion through the CCL and the GDL was addressed in a work of Cruz-Manzo and Greenwood [36]. They considered a Transmission Line Model (TLM) which is indeed a generalization of the Randles circuit accounting for ion transport through the electrode volume [37]. Cruz-Manzo and Greenwood [36] modelled oxygen diffusion through the CCL using a Warburg element, and oxygen diffusion through the GDL using a Kulikovsky

impedance. Their approach led to similar values of the diffusion resistance when one of both impedances (CCL or GDL) was neglected, which can be regarded as possible correlation(s) between them. A similar approach was used by Dierickx et al. [38] who developed a three channel TLM accounting for gas diffusion in addition to ionic transport for the analysis of SOFC impedance spectra.

In the present work, the location of oxygen transport impedance in EEC modeling is discussed. Contrary to the former work of Cruz-Manzo and Greenwood [36], this work is based on Randles-like circuits, *i.e.* thin electrode models. Using TLM-like or Randles-like models impacts the fit quality at high frequencies. The choice between both approaches has thus little or no impact on the considerations about the oxygen transport impedance, which impacts mostly the medium- and low-frequency regions of the spectra. Furthermore, in addition to the location of the diffusion impedance, its expression and more generally its physical meaning are also discussed to identify the most limiting layer for oxygen diffusion. More precisely, two electrical circuits are compared:

- The classical Randles circuit (Figure 2a), with thus the implicit assumption that the CCL (pores or ionomer) is limiting for oxygen diffusion, modeled through a finite Warburg impedance.
- A modified Randles circuit (Figure 2b) where the oxygen diffusion impedance is connected in series to the CCL circuit. This implies that the impact of oxygen diffusion through the GDL is the predominant, while oxygen transport through the CCL is neglected. In this case, the ability of Warburg and Kulikovsky impedances to account for gas diffusion limitations through a passive medium (GDL) is compared.

The EECs were tested on data measured in various operating conditions and for different cells, flow field geometries, and MEA materials. Where necessary, the anode was also considered in the impedance models to improve the fit quality at high frequencies. This choice was consistent with one of our previous works on anode degradation [39].

2. Experimental setup

Four different cells were used in this work: two with straight parallel flow channels (cells A: A1 with segmented current collection, and A2 with regular current collection), one with a single serpentine channel (cell B) and another one with five parallel serpentine channels and segmented current collection (cell C). These cells are shown in Figure 1. All flow-field plates were machined from 316L stainless steel, and gold-coated to improve the electrical contact with the GDL. Different MEAs were used, as detailed in the following.

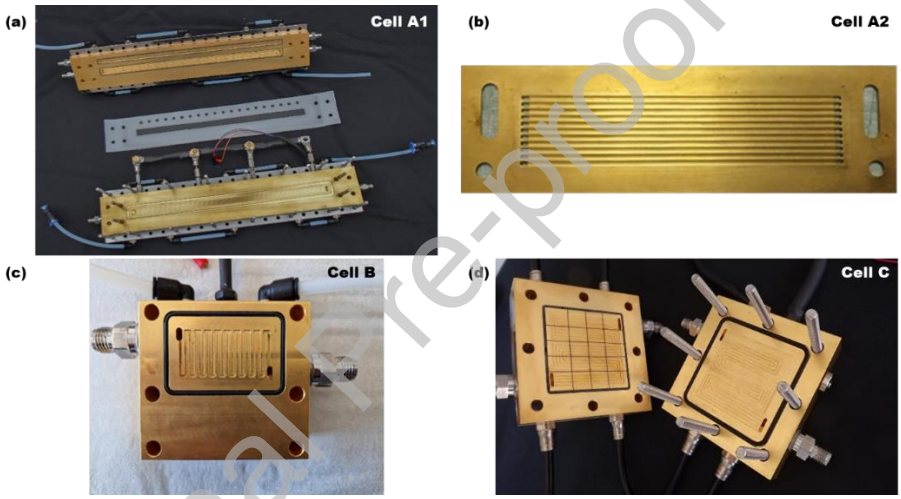

Figure 1.Single cells: (a) segmented cell A1 (1 x 30 cm) with 20 segments at the cathode and 5 linear channels; (b) single cell A2 (98 x 20 mm) with 10 linear channels; (c) single cell B (19 x 38 mm) with 1 serpentine channel; (d) segmented cell C (5 x 5 cm) with 20 segments at the cathode and 5 serpentine channels.

2.1 Cells with straight parallel channels (cells A)

Cell A1 – segmented current collection

Cell A1 had a 30 cm² (300 mm×10 mm) active area, and same flow fields on the anode and cathode sides with 5 parallel straight channels with a width and depth equal to 1 mm and 0.7 mm, respectively. The cathode flow-field plate consists of 20 electrically insulated current collectors allowing to measure local currents and electrode potentials thanks to reference hydrogen electrode (RHE) with a spatial resolution of 1 cm. The detailed architecture and operation principles of this cell are described in several of our previous

works [13,39,40]. Tailored MEAs made by an external supplier with Nafion® XL 100 membranes were used with this cell. The Pt loadings were 0.1 mg_{Pt} cm^{-2} for the anode and 0.3 mg_{Pt} cm^{-2} for the cathode. The gas diffusion layers were 235 µm thick Sigracet 28 BC, compressed to 175 µm using PTFE gaskets to control their thickness.

Cell A2 – regular current collection

Cell A2 had a 19.6 cm^2 (98 mm×20 mm) active area and identical flow fields on the anode and cathode sides with 10 parallel channels. Their width and depth were equal to 1 mm and 0.4 mm, respectively. The MEAs were purchased from an external supplier with a cathode Pt loading estimated to be close to 0.4 mg_{Pt} cm^{-2}, the exact value being not disclosed by the manufacturer. The membrane reference was neither disclosed, but previous works showed that it is a 30 µm thick composite (reinforced) long side-chain polytetrafluoroethylene/perfluorosulfonic acid (PTFE/PFSA) ionomer [41]. 235 µm thick GDLs coated with a Micro Porous Layer (MPL) (SGL 24BC by SGL Carbon) were used on both sides and they were compressed to 200 µm using PTFE gaskets.

2.2 Cells with serpentine channels (cells B and C)

Cell B – regular current collection with a single channel

This cell was designed to operate with a 7.22 cm^2 (19 mm×38 mm) active area MEA. The flow-field plates were identical on both sides, with a single serpentine channel. The width and depth were 1 mm and 0.7 mm, respectively. All the MEAs used with this cell were assembled by hot-pressing (at 135°C and 6.2 MPa, for 3 minutes and 30 seconds), using either a Nafion® 211 (cell B-NR211) or a Nafion® XL 100 membrane (cell B-XL100) and Gas Diffusion Electrodes (GDEs) purchased from HyPlat with a Pt loading of 0.3 mg_{Pt} cm^{-2} on both sides. The GDLs were SGL 28BC compressed to 175 µm using PTFE gaskets.

Cell C - segmented current collection with five parallel channels

Cell C had a 25 cm^2 (50 mm×5 mm) active area, and identical flow-fields on the anode and cathode sides with 5 parallel serpentine channels of width and depth equal to 1

mm and 0.6 mm, respectively. The cathode flow-field plate consists of 20 electrically insulated current collectors allowing the measurement of global and local currents. We used MEAs made by CEA-LITEN by blade-coating the active layers by classical decal transfer onto Gore MX 820.15 membranes as described previously [42]. Commercial carbon-supported (Vulcan carbon; XC72) Pt nanoparticles from TANAKA Kikinzoku Kogyo (50 wt% Pt, TEC10V50E) were used for the catalyst layers with a Pt loading of 0.1 mg_{pt} cm^{-2} at the anode and loadings varying between 0.3 and 0.05 mg_{pt} cm^{-2} at the cathode. These MEAs allowed us to analyze the impact of the cathode Pt loading on the diffusion impedance. The gas diffusion layers were 215 µm thick Sigracet 22 BB, compressed to 173 µm using PTFE gasket. More information about the materials and preparation of these MEA can be found in [43]

2.3 Operating conditions

The operating conditions of each cell are listed in the Table 1. The analyses carried out in the following should thus lead us to general conclusions applying in a relatively wide range of operating conditions, and in different geometries of cells.

Table 1 : Operating conditions of the different cells. The gas inlet RH were always identical on the anode and cathode sides. Detailed description of operating conditions and measuring procedures is given in previous works [13,39,40].

Cell	Fuel cell temperature	Gas Relative Humidity	Air stoichiometry	Hydrogen stoichiometry
A1	80°C	70%	2	1.2
A2	60°C	50%	3	1.5
B	70°C	60%	4	1.5
C	80°C	50%	4	1.5

The impedance data were measured in galvanostatic mode, at 0.5 A cm^{-2} for cell A and B and at 1 A cm^{-2} for cell C -except otherwise stated- with a perturbation amplitude of

10% for frequencies ranging from 10 mHz to 10 kHz, and with 10 data points per decade. Detailed description of operating conditions and measuring procedures is given in previous works [13,39,40].

3. Models

3.1 Electrical Equivalent Circuits

Three EEC configurations were tested to analyze the impedance of the four cells shown in Figure 2: a classical (Figure 2a) and a modified (Figure 2b and c) Randles model standing for the cathode catalyst layer, the membrane and -optionally- the GDL. In these models, R_{hf} corresponds to the sum of to the ionic resistance of the membrane – considered as the main contributor - and other electrical resistances of the MEA and cell components such as the GDL and flow-field plates, as well as the interfaces between them. ORR kinetics in the CCL are modeled through a parallel connection of a charge transfer resistance R_{ct} and a double-layer capacitance C_{dl}, the latter standing for the ability of the porous electrode to store charges in the Electrical Double-Layer (EDL) at the carbon|catalyst-electrolyte interface [44–46]. It was also necessary to consider the anode in the EECs of Figure 2 for a satisfying fit quality with cells A1 and C because a high frequency half-loop (although slight) in the experimental spectra. In this case, the anode was modeled through a parallel connection of a double-layer capacitance $C_{dl,a}$ and a charge transfer resistance $R_{ct,a}$. There is no mass-transport impedance at this electrode due to the high diffusivity coefficient of H_2. When used, the anode EEC is connected in series with the cathode plus membrane circuit (dotted lines in Figure 2) [37].

The difference between the EECs in Figure 2a, b and c lies in the position and type of the oxygen transport impedance: either a finite Warburg element Z_W (1) or an alternative expression derived by Kulikovsky for the GDL Z_K (2). In the Randles circuit Z_W is connected in series with R_{ct} (Figure 2a) implying that oxygen transport limitations are mainly located in the CCL, *i.e*. in the pores or in the ionomer of the CCL. When considering the GDL being

limiting for oxygen transport [13], modified versions of the Randles EEC (Figure 2b and c) were tested in which the oxygen diffusion impedance is connected in series with the CCL circuit and the results obtained with both expressions (Z_W and Z_K) are compared. These oxygen transport impedances are explained in detail in the following. The models include 5 (without anode) to 7 (with anode) parameters.

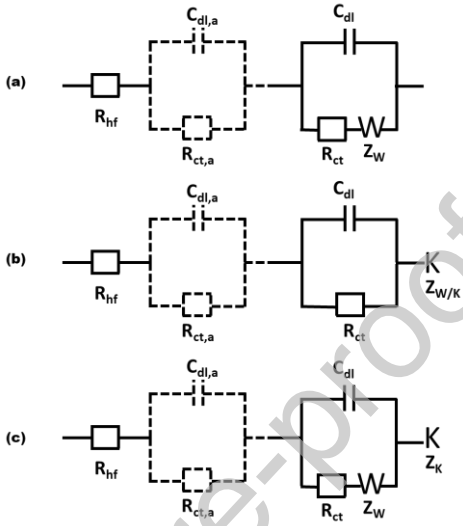

Figure 2. EECs used in this work: the membrane and cathode (solid lines) are modeled either by (a) a usual Randles circuit with the diffusion impedance (Warburg) inside the CCL circuit implying oxygen transport limited by the CCL (pores or ionomer layer), or (b) a modified Randles circuit with the diffusion impedance (Warburg or Kulikovsky) in series with the CCL circuit implying the GDL limiting for O_2 diffusion. Circuit (c) accounts for both oxygen diffusion impedances, the CCL and GDL. The anode is optionally taken into account through a parallel connection of a charge transfer resistance $R_{ct,a}$ and a double-layer capacitance $C_{dl,a}$ (dotted lines).

3.2 Oxygen transport impedance

The most common way to express the oxygen transport impedance in PEMFCs is through a the finite-length Warburg element Z_W [34]. This impedance is derived from Fick's diffusion equations applying to one-dimensional binary diffusion of oxygen and water through a (passive) porous medium. The first boundary condition at the CCL/membrane interface is to suppose a constant oxygen flux governed by the current density (Neumann or second-type boundary condition). The second boundary condition at the CCL/ GDL or GDL/air channel interface is to impose a constant oxygen concentration (Dirichlet or first-type

boundary condition). Other limitations to oxygen transport such as convection [33] (*i.e*. the average molecular flux of oxygen and water is zero in binary diffusion), consumption along the flow fields [47] or contact resistances of the ionomer layer in the CCL [46] might also affect oxygen transport and thus the measured EI spectra. In addition, it should be kept in mind that the low-frequency loop spectrum is generally affected by concentration oscillations induced by the measuring signal perturbation that propagate along the gas channels [30,32]. Finally, the hypothesis of a constant oxygen concentration is reasonable only for relatively high stoichiometric ratios [32,47]. These points are out of the scope of this work and not considered in the Warburg impedance; the reader can refer to the works cited above.

The Warburg impedance is expressed by [34]:

$$Z_{\mathrm{W}} = R_{\mathrm{d}} \frac{\tanh\sqrt{\mathrm{i}\omega\tau_{\mathrm{d}}}}{\sqrt{\mathrm{i}\omega\tau_{\mathrm{d}}}} \qquad (1)$$

where R_{d} is the diffusion resistance (Ω cm²), $\omega = 2\pi\nu$ the angular frequency (rad) and τ_{d} the characteristic diffusion time (s).

Kulikovsky showed that the oxygen diffusion impedance of the GDL should differ from the Warburg expression due to the high double-layer capacitance of the porous CCL, which is responsible of a phase shift between the faradic current density and the oxygen flux. He derived a modified expression of the oxygen diffusion impedance that depends also on the ORR kinetics [35]:

$$Z_{\mathrm{K}} = \frac{Z_{\mathrm{W}}}{1 + \mathrm{i}\omega C_{\mathrm{dl}} R_{\mathrm{ct}}} \qquad (2)$$

with C_{dl} the double-layer capacitance (F cm^{-2}) and R_{ct} the charge transfer resistance (Ω cm²). This expression tends to the Warburg element when C_{dl} tends to zero.

The Randles EEC (Figure 2a) is built with the implicit assumption that the CCL is the limiting layer for oxygen diffusion resulting in the following cell impedance expression [13,24,37]:

$$Z_{\mathrm{CCL}} = R_{\mathrm{hf}} + (\frac{1}{R_{\mathrm{ct}} + Z_{\mathrm{W}}} + \mathrm{i}\omega C_{\mathrm{dl}})^{-1} \quad (3)$$

Note that the index refers to the position of the diffusion impedance in the model. Equation (3) gives the total cell impedance. The same notation system will be applied hereafter. In contrast, the modified Randles EEC (Figure 2b and c) corresponds to the case where the GDL is responsible for oxygen diffusion limitations. The cell impedance in this case writes as:

$$Z_{\mathrm{GDL}} = R_{\mathrm{hf}} + (\frac{1}{R_{\mathrm{ct}}} + \mathrm{i}\omega C_{\mathrm{dl}})^{-1} + Z_{\mathrm{W/K}} \quad (4)$$

With $Z_{\mathrm{W/K}}$ standing for either the classical Warburg impedance Z_{W} (1) or the Kulikovsky impedance Z_{K} (2). Both elements were tested to put forward the impact of the expression of oxygen transport impedance on the identification of the EEC parameters. Kulikovsky's expression was only used in the modified Randles circuit Z_{GDL} (4) because it was derived for mass transport through GDL, *i.e*. diffusive media without a source term, contrary to CCL where oxygen is consumed through the volume.

An EEC with both diffusion impedances was also tested: a Warburg element inside the CCL circuit and a Kulikovsky impedance in series, as shown in Figure 2c. The corresponding cell impedance writes:

$$Z_{\mathrm{CCL+GDL}} = R_{\mathrm{hf}} + (\frac{1}{R_{\mathrm{ct}} + Z_{\mathrm{W}}} + \mathrm{i}\omega C_{\mathrm{dl}})^{-1} + Z_{\mathrm{K}} \quad (5)$$

It turned out that one of both diffusion impedances becomes negligible when trying to identify the impedance parameters from experimental data. That is why only the EECs with one diffusion impedance (eq. (3) and (4)) are used for fitting experimental EIS spectra. The

complete ECC (eq. (5)) is only used for comparison purpose on simulated spectra (section 4.1).

When considering the anode in the impedance model (dotted lines in Figure 2), which was necessary to properly fit the data of cells A1 and C, the cell impedance becomes:

$$Z_{\mathrm{CCL/GDL+a}} = Z_{\mathrm{CCL/GDL}} + \left(\frac{1}{R_{\mathrm{ct,a}}} + \mathrm{i}\omega C_{\mathrm{dl,a}}\right)^{-1} \quad (6)$$

To go one step further into the identification of the limiting layer for oxygen diffusion, and that of the most appropriate impedance model, it is possible to derive both the characteristic diffusion length δ and the effective oxygen diffusion coefficient D_{eff} from the impedance model parameters as shown in [13] [1]. The characteristic diffusion length can be expressed as:

$$\delta = \left(1 + \frac{R_{\mathrm{ct}}}{R_{\mathrm{d}}}\right) \frac{j_{\mathrm{cell}} \tau_{\mathrm{d}}}{4F c^*_{\mathrm{O_2}}} \quad (7)$$

with j_{cell} the cell current density (0.5 A cm^{-2} if not mentioned otherwise), F = 96485 C mol^{-1} the Faraday constant and $c^*_{\mathrm{O_2}}$ the average oxygen concentration at the GDL/gas channel interface assumed constant. The effective oxygen diffusion coefficient is given by:

$$D_{\mathrm{eff}} = \frac{\delta^2}{\tau_{\mathrm{d}}} \quad (8)$$

The above equations are obtained using a macroscopic point of view, i.e. with reference to the MEA flat surface A_{geom}. They are thus suited for diffusion through the pores of the GDL and the CCL. For diffusion through the ionomer film inside the CCL, the reasoning must be made with respect to the microscopic active area, defined as $A_{\mathrm{Pt}} = \gamma A_{\mathrm{geom}}$, with γ the electrode catalytic roughness factor. This implies that the values of δ obtained with equation (7) have to be divided by γ and those of D_{eff} with equation (8) by γ^2.

4. Results

In the following, the use of both configurations of the Randles EEC, i.e. the classical version using the Warburg impedance (Figure 2a) and the modified version with the oxygen diffusion impedance connected in series with the CCL impedance (Figure 2b) are compared to analyze which layer (CCL – pores or ionomer - or GDL) is at the origin of the oxygen diffusion contribution to PEMFC impedance spectra. Section 4.1 presents a theoretical study with the objective to estimate the impedance response that is expected to be observed if one of the considered layers was at the origin of the oxygen diffusion impedance. In section 4.2, the ability of the different versions of the Randles EEC to analyze experimental PEMFC impedance spectra is tested, this for different cell geometries and MEAs operating in various operating conditions. A focus is made in section 4.2.2 on the impact of Pt loading on oxygen diffusion.

4.1 Theoretical study of oxygen transport impedance and PEMFC spectra

In this section, we present a theoretical study on impedance spectra simulated starting from standard values taken from the literature (Table 2). The objective is to estimate the impedance response that is expected to be observed if one of the considered layers (CCL pore/ionomer, GDL) was at the origin of the oxygen diffusion impedance.

More precisely, the diffusion time of the transport impedance τ_d is calculated with eq. (8) starting from the characteristic parameters δ and D_{eff} of the layer at its origin. In addition, we have shown in previous works [13,37] that the diffusion resistance R_{d} can be expressed in a similar way by:

$$R_{\text{d}} = \frac{\delta j R_{\text{ct}}}{4F D_{\text{eff}} c_{\text{O}_2}^{\text{out}}} \qquad (9)$$

With j the current density corresponding to $j_{\text{cell}} = I/A_{\text{geom}}$ with respect to the MEA flat surface A_{geom} when considering oxygen transport through the pores of the GDL or CCL. For

diffusion through the ionomer film, $j = j_{\mathrm{micro}} = j_{\mathrm{cell}}/\gamma$ as transport is considered with respect to the to the active area $A_{\mathrm{Pt}} = \gamma A_{\mathrm{geom}}$. For the present theoretical study, the electrode roughness factor was set to $\gamma = 100$ [48] being a standard value. The charge transfer resistance is linked to the Tafel slope b_{c} via [37]:

$$R_{\mathrm{ct}} = \frac{b_{\mathrm{c}}}{j_{\mathrm{cell}}} \tag{10}$$

Finally, $c_{\mathrm{O_2}}^{\mathrm{out}}$ corresponds to the oxygen concentration at the interface close to the reaction (supposed constant along the MEA surface), *i.e.* the CCL ionomer film/reaction site, CCL pore/ionomer film, or GDL/CCL interface depending on whether the diffusion impedance is located in the CCL (Figure 2a), or in the GDL (Figure 2b). For diffusion through the CCL and GDL pores, the latter is linked to the concentration at the interface with the adjacent previous layer $c_{\mathrm{O_2}}^{\mathrm{GDL}/*}$ by:

$$c_{\mathrm{O_2}}^{\mathrm{CCL/GDL}} = c_{\mathrm{O_2}}^{\mathrm{GDL}/*} - \frac{j_{\mathrm{cell}}\delta_{\mathrm{CCL/GDL}}}{4FD_{\mathrm{eff}}^{\mathrm{CCL/GDL}}} \tag{11}$$

Where $c_{\mathrm{O_2}}^{*}$corresponds to the concentration at the GDL/channel interface, which is estimated using ideal gas law,

$$c_{\mathrm{O_2}}^{*} = \frac{c_{O2\_in}^{*} + c_{O2\_out}^{*}}{2} = \frac{0.21}{2RT}\left((p - p_{\mathrm{vap}}) + (p - p_{\mathrm{sat}})\frac{S_{air} - 1}{S_{air}}\right) \tag{12}$$

with S_{air} being the air stoichiometry, p_{vap} being the vapor pressure and p_{sat} being the saturation vapor pressure [49]. Assuming the ionomer film in the CCL pores at the origin of the diffusion impedance, $c_{\mathrm{O_2}}^{\mathrm{out}}$ in equation (9) has to be calculated using the microscopic approach with respect to the active area $A_{\mathrm{Pt}} = \gamma A_{\mathrm{geom}}$:

$$c_{\mathrm{O_2}}^{\mathrm{ion}} = c_{\mathrm{O_2}}^{\mathrm{CCL}} - \frac{j_{\mathrm{cell}}\delta_{\mathrm{ion}}}{\gamma 4FD_{\mathrm{eff}}^{\mathrm{ion}}} \tag{13}$$

The equations for τ_d (8) and R_{d} (9) are identical for the Warburg and Kulikovsky diffusion impedances. For the numerical simulations of the EI spectra, we considered physically meaningful to use the values related to the CCL (ionomer or pores) in combination with the

Warburg impedance Z_{W} (1) located inside the ORR circuit (Figure 2a), and those related to the GDL with the Kulikovsky Z_{K} (2) impedance connected in series with the ORR circuit (Figure 2b).

Table 2: Theoretical values of the characteristic parameters associated with each layer [50–54]*.*

Layer	C_{dl} [F cm^{-2}]	b_c [V dec^{-1}]	δ [µm]	D_{eff} [m² s^{-1}]	ε [-]
GDL	0.055	0.12	200	$3.2 \times 10^{-5} \times \varepsilon^{2}$	$0.2 - 0.6$
CCL			10	$6.9 \times 10^{-6} \times \varepsilon^{3/2}$	$0.2 - 0.35$
Ionomer			0.01	1.7×10^{-10}	-

Table 3: Theoretical values of the diffusion parameters for the different layers calculated with the values of Table 2 and considering mean values of the porosity ε, i.e. 0.4 for the CCL and 0.275 for the GDL.

Layer	R_d [Ω cm²]	τ_d [s]	$\nu_{\tau d}$ [Hz]
GDL	0.0162	7.81 10^{-3}	20
CCL	0.0043	100.5 10^{-6}	1 544
Ionomer	2.54 10^{-5}	5.88 10^{-7}	27 000

Table 3 shows the values of R_{d}, τ_d and the associated characteristic frequency $\nu_d = 1/(2\pi \times \tau_d)$ of diffusion through each layer using the values of Table 2 and considering mean values of the porosity ε, i.e. 0.4 for the CCL and 0.275 for the GDL. Note that the effective diffusion length is expected to be higher than the associated layer thickness as it depends on the porosity and the tortuosity which are both medium specific. Accounting for these parameters does not affect the order of magnitude of the diffusion impedance parameters (R_{d} and τ_d) of each medium (GDL, CCL pores and ionomer). The effective diffusion length δ is therefore approximated by or compared to the medium thickness through the entire document.

It can be easily seen that the values of the diffusion resistance depend significantly on the layer at its origin and only the one associated with the GDL is on the order of magnitude of those typically identified on PEMFC [13,25,48]; those associated with diffusion through the CCL pores and ionomer are several orders of magnitude lower. Similarly, the characteristic diffusion times and frequencies also depend significantly on the considered layer. Only the frequency associated with diffusion through the GDL ($\nu_d = 20\ Hz$) is situated in the low frequency regime. The frequency associated with the oxygen diffusion though the CCL pores ($\nu_d = 1544\ Hz$) corresponds to the high frequency range, and the one associated with the ionomer layer in the CCL ($\nu_d = 27\ kHz$) pores exceeds the herein applied experimental frequencies (10 mHz - 10 kHz).

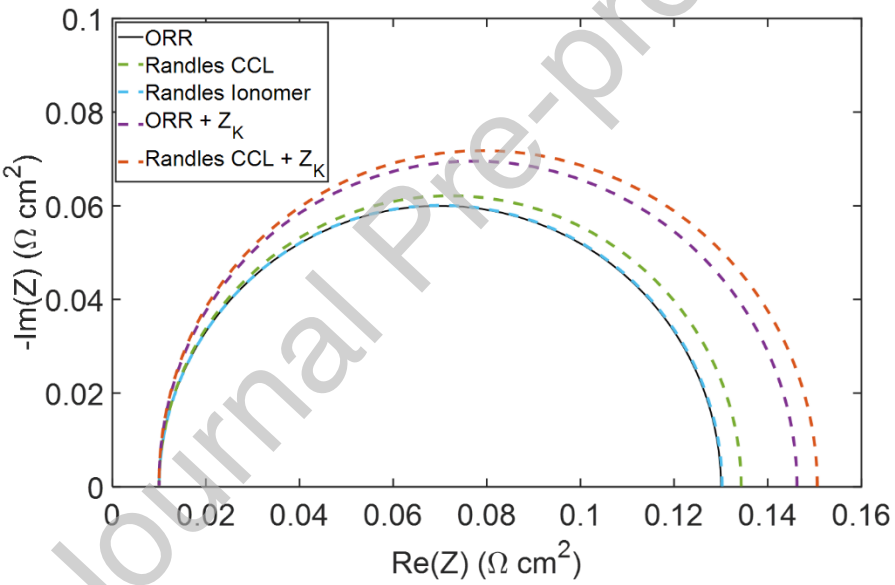

Figure 3. Nyquist plots of the cell impedance spectra simulated starting from the values of Table 2 for frequencies ranging from 10 mHz to 10 kHz. The spectra associated with an origin of diffusion limitations in the CCL (ionomer and pores) are simulated using the classical Randles EEC (eq. (3), Figure 2a), the one supposing the GDL limiting for diffusion is obtained with the modified Randles EEC (eq. (4), Figure 2b).

Figure 3 shows Nyquist plots of the cell impedance simulated starting from the values of Table 2 for frequencies ranging from 10 mHz to 10 kHz. The spectra associated with an origin of diffusion limitations in the CCL (ionomer and pores) are simulated using the

classical Randles EEC (eq. (3), Figure 2a). The one supposing the GDL limiting for diffusion is obtained with the modified Randles EEC (eq. (4), Figure 2b).

These results indicate that -using these parameters values- it is mainly the GDL which is at the origin of the diffusion impedance in the low frequency range of PEMFC impedance spectra. The contribution of diffusion through the CCL pores is significantly lower and that of the ionomer film is negligible in the present conditions. However, this may not be the case with low loaded and/or very active ORR catalysts increasing the oxygen flux per active catalyst site and thus the associated effective resistance [42,45]. As a consequence, the physically most consistent EEC would therefore be a series connection of an ORR circuit with the Kulikovsky diffusion impedance Z_K, as depicted in Figure 2b, or alternatively, a classical Randles circuit completed by a Kulikovsky diffusion impedance Z_K (Figure 2c) in order to include diffusion limitations in the CCL pores. Note that the EEC with two diffusion impedance elements adds two impedance parameters to the model and therefore possible correlations between them. As a result, there will be a strong risk of lowering the sensitivity for their estimation starting from experimental data using this circuit.

We emphasize that the herein-used oxygen transport impedance expressions consider only 1D Fickian diffusion. The objective was to discuss the physically most meaningful position and expression of the diffusion impedance in the cell equivalent electrical circuit. Other phenomena such as convection [33], consumption along the flow fields [47], or thin-film phenomena associated to the ionomer film within the CCL pores, i.e. the contact resistance with the CCL pores [46], might as well play a significant role in the overall oxygen transport. They are neglected in the impedance expressions that are analyzed here, the objective of this work being only to discuss the role of oxygen diffusion limitations in PEMFC impedance spectra and the layer at their origin.

Finally, the Nyquist plot of the simulated cell impedances in Figure 3 exhibits one unique loop. We conclude that the separation between the loops associated with the ORR kinetics and diffusion which is usually observed in experimental EI spectra for PEMFCs supplied with

air (e.g. experimental spectra in this document) might be due to either other transport phenomena than diffusion, as mentioned above (convection, interface phenomena…), or linked with measurement artefacts due to current-induced concentration oscillations [30–32]. The impact of these artefacts is discussed below when interpreting local impedance data (section 4.2).

4.2 Oxygen diffusion impedance model analyses from experimental data

4.2.1 Cell A1 – linear cell with segmented current collection

Global impedance spectrum

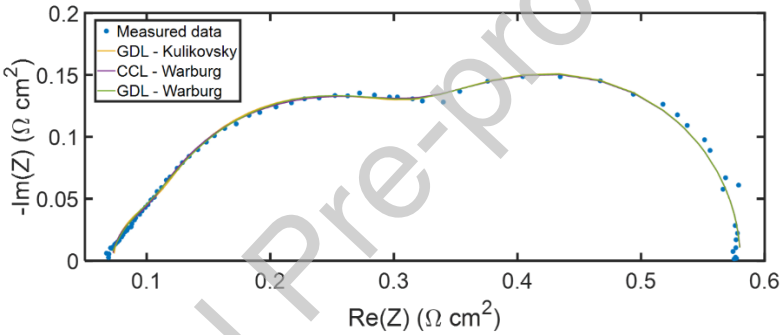

Figure 4. Experimental Nyquist diagram measured in operando (0.5 A cm^{-2} and 0.68 V, under H_2/air) with cell A1 in the operation conditions described in section 2.3 and fitting curves obtained with the different EECs depicted in Figure 2 [39].

Figure 4 shows the global impedance spectrum measured with cell A1 (dots) in the operating conditions described in section 2.3. The fitting curves obtained with the EECs including the anode (Figure 2a and b) and corresponding impedance expressions eq. (6) are given by the solid lines. The identified intrinsic parameters are shown in Table 4, on which the impact of the location (CCL or GDL) and expression (Warburg or Kulikovsky) of the oxygen diffusion impedance will be discussed in the following.

Table 4: Parameters estimated with the EECs in Figure 2 for the experimental data measured with cell A1 (Figure 4). Comparison is made between the location (CCL or GDL) and the expression (Z_W or Z_K) of the diffusion

impedance. Kulikovsky expression was derived for O_2 transport through the GDL and is thus exclusively used for the modified Randles EEC (Figure 2b).

Model	R_{hf} [Ω cm²]	R_{ct} [Ω cm²]	C_{dl} [mF cm^{-2}]	R_d [Ω cm²]	τ_d [s]	$R_{ct,a}$ [Ω cm²]	$C_{dl,a}$ [F cm^{-2}]
Warburg CCL	0.072	0.212	19.5	0.262	0.128	0.033	0.011
Warburg GDL	0.068	0.169	31.2	0.320	0.137	0.024	0.020
Kulikovsky GDL	0.073	0.168	25.4	0.296	0.137	0.042	0.011

It can be seen, that neither the location nor the expression of the oxygen transport impedance has a significant impact on the fitting curves which are identical. However, the estimated values of the impedance parameters depend on the chosen EEC: both, the expression of the diffusion impedance (Z_W or Z_K) and its location in the cell EEC -whether included in the CCL circuit eq. (3) or connected in series eq. (4)- impact significantly the parameters associated with mass transfer, i.e. R_d and τ_d (up to about 20%), but also those related to the ORR kinetics (up to 60%), *i.e.* the charge transfer resistance R_{ct} and double-layer capacitance C_{dl}. Connecting the diffusion impedance in series with the CCL circuit (GDL configuration, eq. (4)) increases the values of the parameters of the oxygen diffusion impedance (R_d and τ_d), in favor of those associated with the ORR kinetics (i.e. lower charge transfer resistance and higher double-layer capacitance). The expression of the diffusion impedance (Warburg or Kulikovsky) affects mainly the double-layer capacitance C_{dl} and the diffusion resistance R_d and to a lower extend, R_{ct}. This could be expected since the Kulikovsky impedance Z_K eq. (2) is linked to the Warburg impedance Z_W, through the ORR kinetic parameters R_{ct} and C_{dl}. The high-frequency resistance R_{hf} is only slightly impacted (less than 6%). This was expected since mass transport affects mostly the low frequency part of the spectrum: the characteristic frequency associated with the oxygen diffusion impedance parameters in Table 4 is about $\upsilon_d = 1/(2\pi\tau_d) \approx 1.2\ Hz$.

More surprisingly, the anode impedance parameters depend as well on the location and expression of the oxygen transport impedance (variations up to about 80%), although the impedance of this electrode manifests itself mostly at higher frequencies than those associated with oxygen diffusion: using the values in Table 4, the characteristic frequency of the parameters associated with the HOR kinetics is about $\upsilon_{ct,a} = 1/(2\pi R_{\mathrm{ct,a}} C_{\mathrm{dl,a}}) \approx 400\,Hz$ which is significantly higher than that of oxygen diffusion ($\upsilon_d \approx 1.2\,Hz$). A possible explanation could be that the correlation is made through the impedance parameters associated with the ORR kinetics as discussed above. The characteristic frequency of the ORR kinetics referring to the parameters in Table 4 is $\upsilon_{ct} = 1/(2\pi R_{\mathrm{ct}} C_{\mathrm{dl}}) \approx 40\,Hz$ which is situated between those of the HOR and oxygen diffusion.

To summarize at this point, both the location and the expression of the diffusion impedance impact the values estimated for all the impedance model parameters, and those associated with oxygen diffusion and ORR kinetics to the highest extent. However, all configurations lead to values of the same orders of magnitude and in agreement with former estimations made for these data [39], as well as to similar fit quality, so that no conclusion can be drawn, so far, on the most appropriate EEC model in terms of oxygen diffusion impedance.

To go one step further into the identification of the limiting layer for oxygen diffusion, and that of the most appropriate impedance model, the characteristic diffusion length δ and the effective diffusion coefficient D_{eff} were estimated for each of the above EEC with eq. (7) and (8), respectively. The results obtained with the impedance data of Table 4 are depicted in Table 5.

Table 5: Oxygen diffusion parameters obtained from the impedance parameters in Table 4.

Model	**Warburg CCL - ionomer A_{Pt}**	**Warburg CCL – pores A_{geom}**	**Warburg GDL**	**Kulikovsky GDL**
δ [µm]	222	489	444	454
D_{eff} [10^{-6} m² s^{-1}]	0.38	1.87	1.44	1.50

The values in the columns referring to the GDL configuration (Warburg and Kulikovsky GDL) and to diffusion through the CCL pores (Warburg CCL – pores) are obtained when adopting the macroscopic approach with respect to the MEA flat surface A_{geom}. In all cases, the values obtained for δ are of the order of the thickness typically given for GDL (some hundreds of µm [55,56]) rather than that of a CCL (about 10 µm [57,58]). Furthermore, the values of D_{eff} are of the same order than that of oxygen diffusion in vapor phase through the GDL (Table 6).

The values given in the first column in Table 5 (Warburg CCL ionomer) are obtained starting from the values obtained with the classical Randles EEC and adopting the microscopic approach with respect to the active surface A_{Pt} assuming an electrode roughness factor $\gamma = 100$ [48]. Note that the diffusion parameters which are linked with the GDL EEC (Warburg and Kulikovsky) cannot be used for similar macroscopic to microscopic downscaling since the ionomer film is located within the CCL. The values of the effective diffusion coefficient D_{eff} = 0.38 10^{-6} m^2 s^{-1} and the diffusion length δ = 222 µm are closer to those of a GDL than those expected for the ionomer film in the CCL (0.01 µm – 0.1 µm [28,46,59] for its thickness and about 10^{-10} m^2 s^{-1} for the diffusion coefficient of oxygen in the ionomer [54]). This confirms that the CCL (pores or ionomer film) is not the main contributor to the oxygen diffusion impedance associated with the PEMFC spectrum in Figure 4.

Table 6: Reference values of the effective diffusion coefficient of oxygen in different layers and phases [50–54].

Layer	**Phase**	$D_{\mathrm{eff}} = D\varepsilon^m$ **[m² s^{-1}]**	**Porosity ε [-]**	D_{eff} **[m² s^{-1}]**
GDL	Vapor	$3.2\ 10^{-5} \times \varepsilon_{GDL}^2$	0.2 – 0.6	$1.3\ 10^{-6}$ – $1.15\ 10^{-5}$
	Liquid	$1.2\ 10^{-10} \times \varepsilon_{GDL}^2$		$4.8\ 10^{-12}$ – $4.3\ 10^{-11}$

Catalyst layers	Vapor	$6.9\ 10^{-6} \times \varepsilon_{GDL}^{3/2}$	0.2 – 0.35	$6.2\ 10^{-7}$ – $1.4\ 10^{-6}$
	Liquid	$1.2\ 10^{-10} \times \varepsilon_{GDL}^{3/2}$		$1.1\ 10^{-11}$ – $2.5\ 10^{-11}$
Ionomer (Nafion)	Liquid	-	-	$1.7\ 10^{-10}$

From these results, one can conclude that the GDL is the main origin of the diffusion impedance identified from the spectrum of Figure 4, with a possible minor contribution of the CCL. The choice of the diffusion impedance model (Warburg eq. (1) or Kulikovsky eq. (2)) only slightly impacts the estimate of the diffusion characteristics. However, based on the interpretation that the GDL is the main contributor to the diffusion impedance, the physically most consistent EEC would therefore be a series connection of an ORR circuit with the Kulikovsky diffusion impedance Z_K, as depicted in Figure 2b.

It must be reminded that the low frequency loop in the global spectrum is affected by concentration oscillations induced by the measuring signal [30–32] and hence the impedance parameters identified from the graph in Figure 4. Their impact is enhanced the lower the gas concentration and can thus be attenuated by increasing the gas stoichiometry. An alternative consists in analyzing local EI spectra measured on the first segments i.e. near the oxygen inlet, which is discussed below.

Local impedance spectra

Cell A1 being segmented, with 20 electrically insulated current collectors, the approach described above was completed using the spectra measured on the first five segments corresponding to the air inlet/hydrogen outlet (Figure 5).

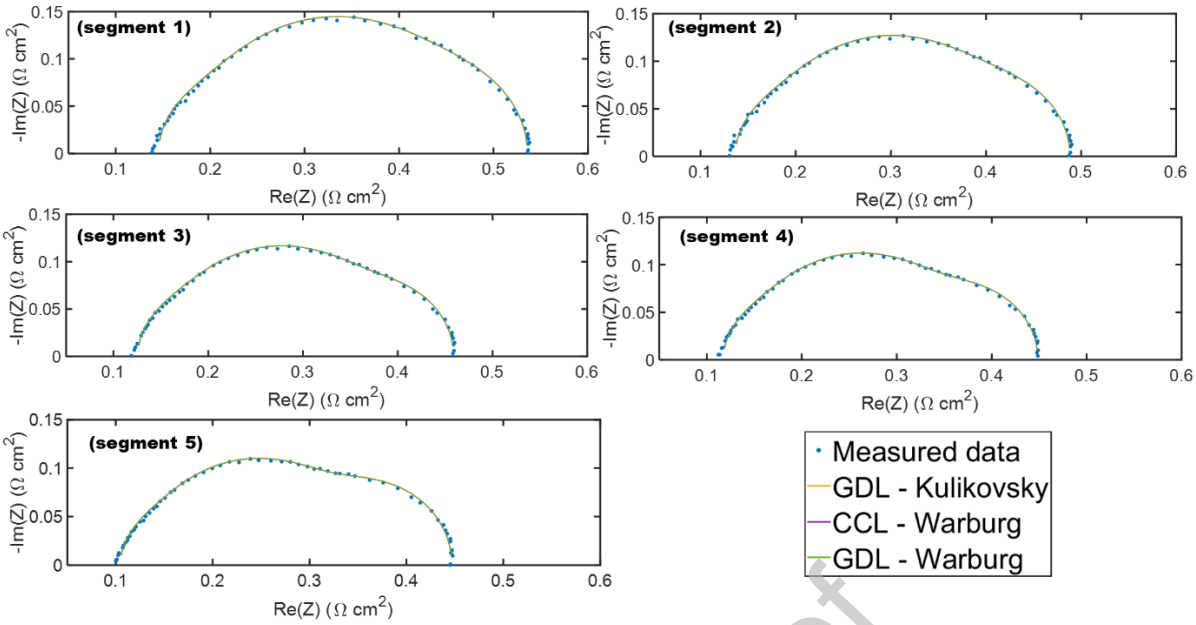

Figure 5. Nyquist plots of data measured on the first 5 segments (air inlet/hydrogen outlet) of cell A1 (Figure 1a) at 0.5 A cm^{-2} (H_2/air) in the operation conditions described in section 2.3. The fitting curves were obtained with the EECs depicted in Figure 2.

As can be seen in Figure 5, the low frequency loop increases with the segment number (along the air channel) and the separation between the intermediate and low frequency loops becomes as well more pronounced. One contribution is certainly linked to oxygen depletion, but current density-induced oxygen concentration oscillations might play a major role [30–32,47]. These observations, completed by the fact that their evolution with the segment number depends on the flow field geometry (less uniform for serpentine channels, Figure 8) argue in favor of this hypothesis.

Table 7. Parameters estimated by fitting the experimental data in Figure 5 with the EECs in Figure 2 a) (CCL configuration) and b) (GDL configuration). A comparison is made between the diffusion impedance position (CCL or GDL) and expression (Warburg and Kulikovsky).

Segment \ Model		R_{ct} [Ω cm²]	C_{dl} [mF cm^{-2}]	R_d [Ω cm²]	τ_d [s]
Segment 1	**Warburg CCL**	0.256	10.9	0.076	0.035
	Warburg GDL	0.227	13.0	0.114	0.037

	Kulikovsky GDL	0.237	12.1	0.095	0.037
Segment 2	**Warburg CCL**	0.223	12.9	0.079	0.041
	Warburg GDL	0.196	15.7	0.113	0.044
	Kulikovsky GDL	0.200	14.4	0.096	0.043
Segment 3	**Warburg CCL**	0.180	16.4	0.100	0.050
	Warburg GDL	0.203	14.4	0.084	0.048
	Kulikovsky GDL	0.180	16.4	0.100	0.050
Segment 4	**Warburg CCL**	0.194	15.6	0.095	0.057
	Warburg GDL	0.168	19.9	0.126	0.060
	Kulikovsky GDL	0.170	17.9	0.112	0.059
Segment 5	**Warburg CCL**	0.187	16.8	0.117	0.064
	Warburg GDL	0.158	22.8	0.152	0.068
	Kulikovsky GDL	0.160	20.0	0.136	0.067

The intrinsic parameters obtained by fitting the experimental spectra in Figure 5 using the EECs in Figure 2a and b are depicted in Table 7. For simplicity, only the parameters the most impacted by the choice of the model are shown. As the LF loop and thus the identified impedance parameters might be affected by oxygen concentration oscillations as previously discussed, their evolution along the channel length, i.e. over the first five segments, is not discussed. The discussion focuses instead on the impact of the position and expression of the oxygen diffusion impedance inside the cell EEC as for the analysis of the global spectrum, with a particular attention on the spectrum measured on the first segment, which is expected to be less affected by these measuring artefacts.

As for the global impedance spectrum in Figure 4, all the tested EECs fit satisfyingly and equally well the local spectra, independently of the location (CCL or GDL) or the expression (Warburg or Kulikovsky) of the oxygen diffusion impedance, but the values of all parameters depend on the chosen model.

To conclude about the layer at the origin of the diffusion impedance, the characteristic diffusion length δ and the effective diffusion coefficient D_{eff} have been determined for the first five segments starting from the values of R_{d} and τ_d in Table 7 and using equations (7) and (8) with a macroscopic (with respect to the MEA flat surface A_{geom}) and a microscopic point of view (with respect to the active area $A_{\text{Pt}} = \gamma A_{\text{geom}}$). They are displayed in Table 8. The same observation is obtained for all segments: the values obtained for δ are of the order of a GDL thickness and those of D_{eff} are of the order of oxygen diffusion in vapor phase through this layer (Table 6), independently if using the macroscopic or microscopic approach. The increase of δ along the segments is consistent with the increase of the LF loop of the impedance spectra. Nonetheless, the results obtained on all segments, including the first one which is expected to be less subjected to measuring artefacts, lead to the same conclusions.

In summary, the analysis of the local impedance data confirms the conclusions drawn from the global spectrum regarding the layer being at the origin of oxygen diffusion limitations: the main contribution seems to come from the GDL, or both the GDL *and* the CCL, the latter with a significant lower contribution. Based on these observations, the most appropriate EEC for interpreting the impedance spectra measured with cell A1 would be the modified Randles EEC in GDL configuration, i.e. with a Kulikovsky diffusion impedance in series with the ORR circuit (Figure 2b).

Table 8. Characteristic diffusion parameters obtained with the impedance parameters of the first 5 segments of cell A1 given in Table 7.

Segment \ Model		**Warburg CCL - ionomer** A_{Pt}	**Warburg CCL – pores** A_{geom}	**Warburg GDL**	**Kulikovsky GDL**
Segment 1	**δ [µm]**	185	239	174	196
	D_{eff} **[m² s^{-1}] 10^{-6}**	0.97	1.62	0.81	1.04
Segment 2	**δ [µm]**	186	251	192	209

	D_{eff} [m² s^{-1}] 10^{-6}	0.84	1.53	0.84	1.02
Segment 3	**δ [µm]**	192	270	215	230
	D_{eff} [m² s^{-1}] 10^{-6}	0.77	1.52	0.9	1.05
Segment 4	**δ [µm]**	197	291	237	252
	D_{eff} [m² s^{-1}] 10^{-6}	0.68	1.50	0.93	1.07
Segment 5	**δ [µm]**	180	291	243	255
	D_{eff} [m² s^{-1}] 10^{-6}	0.51	1.32	0.86	0.97

4.2.2 Other cells – impact of cell geometry and MEA composition

The following sections present the results of equivalent analyses of data measured on the other cells described in section 2 in comparison to those of cell A1. The objective is to test the validity of the former conclusions about the most appropriate EEC to account for oxygen diffusion limitations in PEMFC impedance spectra (modified Randles EEC with Kulikovsky impedance) for different cell geometries and MEA compositions. A focus is made on the data measured on MEA with different Pt loadings at the cathode, which could give a hint on the impact of the role of the ionomer layer for oxygen transport limitations.

Cell geometry and MEA composition (cells A2 and B)

This section addresses the role of:

- cell geometry, more precisely MEA surface;
- flow field configuration (5 straight parallel channels for cells A1 and A2, 1 serpentine channel for cell B);
- MEA type (CCM for cell A2 and GDEs hot-pressed on different membranes) for cell B.

Figure 6 shows the EI spectra measured on each cell at 0.5 A cm^{-2} (under H_2/air) in the operation conditions given in section 2.3 and the fitting curves obtained with the EECs in Figure 2a and b (solid lines only). As shown above, the anode impacts the spectra at high

frequencies only and has negligible impact on the conclusions about the diffusion impedance. It is therefore neglected in the ECCs for the present study to reduce the model parameters.

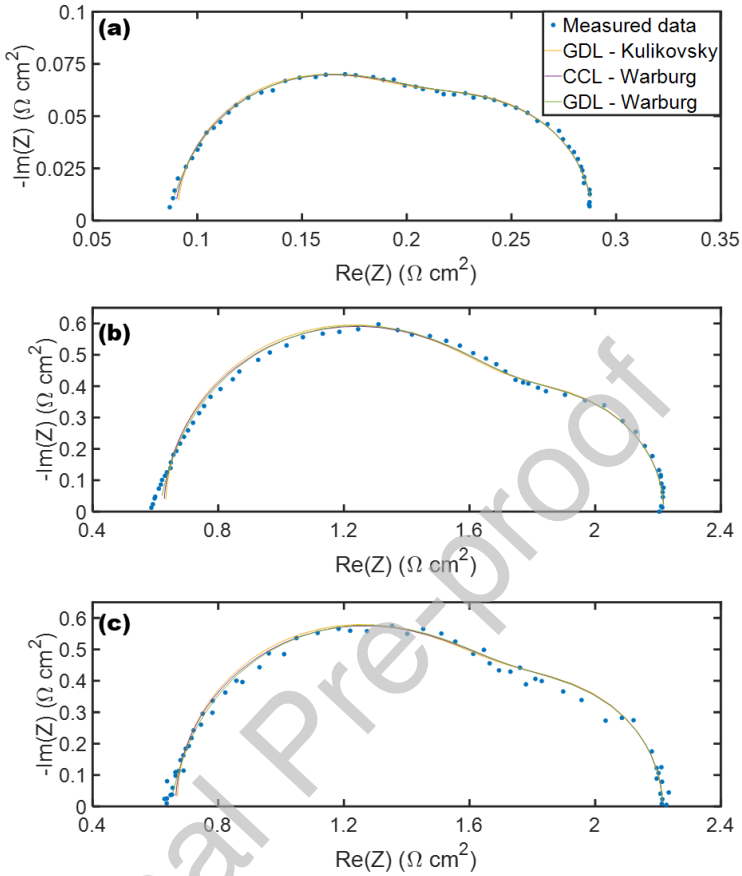

Figure 6. Nyquist diagrams of the impedance data measured at 0.5 A cm^{-2} (under H_2/air) with (a) cell A2 [13]*, (b) cell B - NR211 and (c) cell B - XL100 in the operation conditions given in section 2.3 and fitting curves obtained with the different EECs depicted in Figure 2a and b (solid lines). The anode is neglected.*

The identified impedance parameters are shown in Table 9. All EECs yield values consistent with those typically observed for such MEAs [13,25,48].

Cells A1 and A2 have comparable geometry and same flow field configuration (5 parallel straight channels), cell A2 used a commercial MEA purchased from another provider with lower active area. The anode loop is completely overwhelmed by that of the cathode in the Nyquist plot of cell A2, which confirms that it is wise to neglect it in the cell EEC. The fit of this data serves thus as complementary validation of the tested Randles-type EECs in Figure 2 for standard commercial MEAs.

The MEAs in cell B are made by hot-pressing using GDEs. It is expected that their electrode thickness is higher than that of commercial MEAs which could lead to the appearance of a straight line at high frequencies in the Nyquist plot. This shape is associated with ion conduction limitations trough the CCL volume and could be accounted for in EEC modeling by the use of TLM-like circuits [13,36,39]. However, this is out of the scope of this work as this phenomenon impacts the spectra only at higher frequencies than those associated with oxygen diffusion impedance. Ion conduction is thus neglected in the present EEC model for the sake of simplicity. The difference between cells B1 and B2 is the membrane type: Nafion 211 for cell B1 and Nafion XL 100 for cell B2 (not disclosed for cell A2). As expected, a difference is observed mainly for the value of the high frequency resistance R_{hf} associated with the ionic conductivity of the membrane. The other parameters are similar.

Table 9. Parameters estimated by fitting the experimental data in Figure 6 with the EECs in Figure 2a) and b) (anode neglected, solid lines). Comparison is made between the diffusion impedance position (CCL or GDL) and expression (Warburg and Kulikovsky).

Cell\ Model		R_{hf} [Ω cm²]	R_{ct} [Ω cm²]	C_{dl} [mF cm^{-2}]	R_d [Ω cm²]	τ_d [s]
Cell A2 [13] **– 5 parallel channels, membrane not disclosed**	**Warburg CCL**	0.089	0.124	30.2	0.075	0.067
	Warburg GDL	0.084	0.104	41.0	0.100	0.073
	Kulikovsky GDL	0.091	0.106	33.9	0.092	0.070
Cell B1 – 1 serpentine channel, Nafion 211	**Warburg CCL**	0.664	1.062	2.29	0.488	0.050
	Warburg GDL	0.637	0.948	2.86	0.629	0.053
	Kulikovsky GDL	0.669	0.964	2.47	0.579	0.070
Cell B2 – 1 serpentine channel, Nafion XL 100	**Warburg CCL**	0.627	1.101	2.09	0.491	0.056
	Warburg GDL	0.602	1.001	2.55	0.615	0.058
	Kulikovsky GDL	0.632	1.016	2.25	0.569	0.056

Concerning the impact of the position (CCL or GDL) and the expression (Z_W or Z_K) of the oxygen diffusion impedance in the cell EEC, the same trends are observed as for cell A1: all configurations lead to values of the same orders of magnitude, as well as to similar fit quality, so that no conclusion can be drawn so far on the most appropriate EEC model for the diffusion impedance.

To conclude about the most appropriate EEC configuration, the characteristic diffusion parameters, i.e. δ and D_{eff}, have been determined with eq. (7) and (8), respectively. Their values are given in Table 10 when considering the oxygen flux relative to the MEA flat

surface. The results obtained when accounting for the catalytic active area $A_{\mathrm{Pt}} = \gamma A_{\mathrm{geom}}$ are not shown here as they are clearly out of the range of those associated with the ionomer film in the CCL wich is consistent with the observations on the data of cell A1.

Table 10. Characteristic diffusion parameters obtained with the impedance parameters of cells A2, B1 and B2 given in Table 9.

Cell \ Model		Warburg CCL	Warburg GDL	Kulikovsky GDL
Cell A2 – 5 parallel channels, membrane not disclosed	**δ [µm]**	309	260	265
	D_{eff} [m² s^{-1}] 10^{-6}	1.42	0.92	0.99
Segment 2 Cell B1 – 1 serpentine channel, Nafion 211	**δ [µm]**	294	247	252
	D_{eff} [m² s^{-1}] 10^{-6}	1.75	1.15	1.25
Cell B2 – 1 serpentine channel, Nafion XL 100	**δ [µm]**	340	281	293
	D_{eff} [m² s^{-1}] 10^{-6}	2.06	1.40	1.51

For all tested cells, the values identified for the characteristic diffusion length are of the order of the GDL thickness [55,56], while the effective diffusion coefficient is of the order of oxygen diffusion in vapor phase through this layer (Table 6) which confirms the observations made on the data measured with cell A1.

Independently of the cell geometry, it seems that it is most likely oxygen diffusion in vapor phase in the pores of the GDL (or the GDL and the CCL) that is at the origin of the diffusion impedance. The most appropriate EEC would thus be the modified Randles model with a Kulikovsky diffusion impedance connected in series with the CCL circuit as depicted in Figure 2b.

Cathode Pt loading (cells C)

This section presents the results obtained when applying the EECs to fit the data measured on MEAs with different cathode Pt loadings situated between 0.05 mg_{Pt} cm^{-2} and 0.3 mg_{Pt} cm^{-2}. The MEA were used in cell C having 5 parallel serpentine flow fields and segmented current collection (Figure 1d).

Figure 7 shows the global impedance spectra measured for each MEA at 1 A cm^{-2} (under H_2/air) in the operation conditions given in section 2.3 and the fitting curves obtained with the EECs in Figure 2a and b, including the anode. It can directly be seen that the global cell impedance increases when lowering the cathode Pt loading, suggesting additional limitations for low Pt-loaded cathodes.

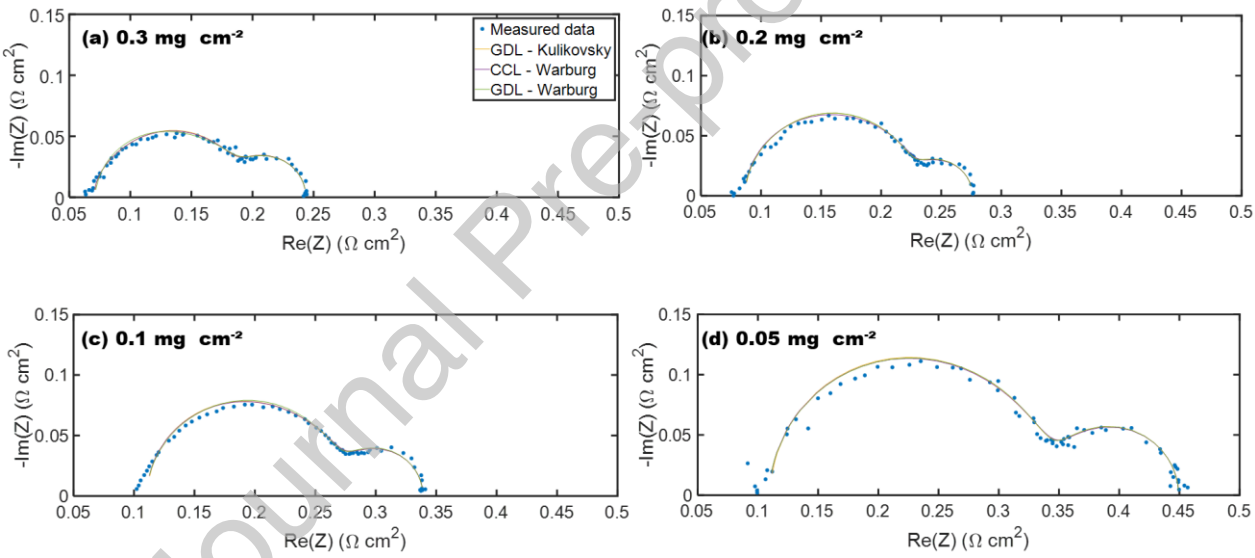

Figure 7. Nyquist diagrams of the impedance data measured at 1 A cm^{-2} (H_2/air) with cell C using MEAs with different Pt loadings at the cathode in the operation conditions given in 2.3 and fitting curves obtained with the EECs depicted in Figure 2a and b (anode included). The cell voltages during characterization are: (a) 0.60 V; (b): 0.55 V; (c): 0.51 V et (d): 0.45 V.

Table 11 shows the values of the high frequency resistance (R_{hf}), the ORR (R_{ct}, C_{dl}) and the diffusion impedance parameters (R_d, τ_d) for each cathode Pt loading identified from the global impedance spectra in Figure 7 with the EEC in GDL configuration using the Kulikovsky diffusion impedance and considering the anode (Figure 2 b). All EEC configurations lead to similar values and their influence on the identified impedance parameters is identical to that

of the other cells. The values obtained using the Warburg element instead of the Kulikovsky impedance were published in a previous work [43]. Discussion is therefore directly made on the physically most relevant EEC.

Table 11 : Values of the impedance parameters (except anode) of each cathode Pt loading form the global impedance spectra of cell C (Figure 7) with the EECs in GDL configuration using the Kulikovsky diffusion impedance and considering the anode (Figure 2 b).

Cathode Pt loading	R_{hf} [Ω cm²]	R_{ct} [Ω cm²]	C_{dl} [mF cm^{-2}]	R_d [Ω cm²]	τ_d [s]
0.3 mg cm^{-2}	0.071	0.072	13.3	0.065	0.042
0.2 mg cm^{-2}	0.088	0.094	7.1	0.056	0.040
0.1 mg cm^{-2}	0.112	0.104	5.6	0.078	0.040
0.05 mg cm^{-2}	0.116	0.214	1.7	0.092	0.047

It can be seen that the high frequency resistance R_{hf} increases from 0.071 Ω cm² to 0.116 Ω cm², when lowering the Pt loading from 0.3 mg_{Pt} cm^{-2} to 0.05 mg_{Pt} cm^{-2}. Same membrane, GDL, anode catalyst layer composition and bipolar plates being used in all cases, indicating that the origin of this trend might be linked to the CCL and more precisely the ionomer film : the theoretical study in section 4.1 indicates that the associated oxygen transport limitations might be situated at high frequencies and they are expected to increase when lowering the Pt loading [46]. This trend agrees with former observations in the literature stipulating that the electrode oxygen transport impedance is inversely proportional to platinum loading or, equivalently, platinum surface area [60–62]. Note that other phenomena may contribute to the increase of R_{hf}: EIS measurements are made at 1 A cm^{-2}, implying a lower cell voltage and thus higher temperature when decreasing the Pt loading. To go further, it would be interesting to repeat the EI measurements at constant cell voltage. In addition, the charge-transfer resistance R_{ct} increases from 0.072 Ω cm² to 0.214 Ω cm² while the double-layer capacity C_{dl} decreases from 13.3 to 1.7 mF cm^{-2}, which is consistent with slower ORR

apparent kinetics for lower Pt surface area electrodes. Finally, the oxygen diffusion resistance R_d increases from 0.065 Ω cm² to 0.092 Ω cm², for a constant diffusion time τ_d when lowering the Pt loading which agrees with the increase of the low frequency loop of the spectra.

Table 12. Characteristic diffusion parameters identified form the impedance spectra of cell C (Figure 7) with the EECs depicted in Figure 2a and b including the anode.

Cathode Pt loading \ Model		**Warburg CCL - ionomer A_{Pt}**	**Warburg CCL – pores A_{geom}**	**Kulikovsky GDL**
0.3 mg cm^{-2}	**δ [μm]**	207	349	312
	D_{eff} [m² s^{-1}] 10^{-6}	1.04	2.96	2.32
0.2 mg cm^{-2}	**δ [μm]**	299	437	381
	D_{eff} [m² s^{-1}] 10^{-6}	2.22	4.76	3.60
0.1 mg cm^{-2}	**δ [μm]**	249	381	325
	D_{eff} [m² s^{-1}] 10^{-6}	1.57	3.69	2.66
0.05 mg cm^{-2}	**δ [μm]**	524	672	541
	D_{eff} [m² s^{-1}] 10^{-6}	6.00	9.91	6.31

Table 12 shows the diffusion parameters (δ and D_{eff}) identified from the spectra in Figure 7 using either the diffusion impedance (Warburg) inside the ORR circuit (classical Randles model, Figure 2a) or when connecting the diffusion impedance (Kulikovsky) in series with the ORR circuit (GDL configuration, Figure 2b). The values in the columns referring to the EEC configurations with the diffusion impedance linked to the GDL (Kulikovsky GDL) and CCL pores (Warburg CCL – pores) are obtained when adopting the macroscopic approach with respect to the MEA flat surface A_{geom}. Those in the first column (Warburg CCL ionomer) are obtained starting from those identified with the classical Randles circuit (Figure 2a) and

adopting the microscopic approach with respect to the active Pt area A_{Pt}, this time using the electrode roughness factor γ identified experimentally (14) for each MEA ($\gamma = 14,\ 26,\ 60,\ 71$ for the Pt loadings 0.05, 0.1, 0.2, 0.3 mg cm^{-2}, respectively).

$$\gamma = ECSA\ (m^2/g) * Pt\ loading\ (g/m^2) \qquad (14)$$

Independently of the EEC, the values of the diffusion parameters show a large dispersion but tend to increase globally when lowering the Pt loading, more pronounced for δ than for D_{eff}. This is consistent with an increase of the overall impedance spectrum including the LF loop and the increase of R_d when decreasing the cathode Pt loading. On a physical point of view, this is however in contrast with thinner electrodes when lowering the Pt loading [43] indicating that the diffusion impedance contribution at low frequencies might not be linked to the cathode, at least not majorly. As for all other cells and MEAs the values identified for the characteristic diffusion length δ are of the order of the GDL thickness [55,56], while the effective diffusion coefficient D_{eff} is of the order of oxygen diffusion in vapor phase through this layer (Table 6).

This leads to the same conclusion as above: the GDL seems to be the main origin of the oxygen diffusion impedance, with a possible minor contribution of the CCL pores or the ionomer film, both however overwhelmed by the GDL contribution. On a modeling point of view, the physically most appropriate EEC for analyzing the impedance data measured on cell C is thus again the modified Randles EEC in GDL configuration with a Kulikovsky impedance in series with the ORR EEC (Figure 2b). The ionomer film inside the CCL might contribute to the high frequency resistance, its exact contribution is difficult to identify at this point.

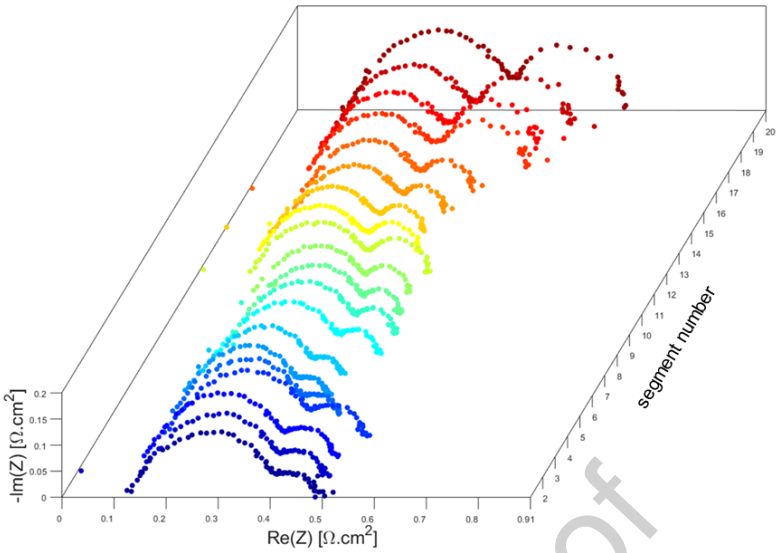

Figure 8. Nyquist plots of local impedance spectra measured on cell C (Figure 1d) at 1 A cm^{-2} (H_2/air) in the operation conditions described in section 2.3. The data corresponds to a MEA with cathode Pt loading of 0.05 mg_{Pt} cm^{-2}. Segment 1 corresponds to the air inlet/hydrogen outlet and segment 20 to the air outlet/hydrogen inlet. It must be noted that the cell segments operate at different current density since the cell voltage is homogeneous: the local operating points are all different.

Figure 8 shows the local impedance spectra measured on cell C for the MEA with the lowest cathode Pt loading, i.e. 0.05 mg_{Pt} cm^{-2} (global spectrum in Figure 7d). Segment 1 corresponds to the air inlet/hydrogen outlet and segment 20 to the air outlet/hydrogen inlet. The purpose is to compare the impact of the flow field geometry (straight for cell A1 and serpentine for cell C) on the evolution of the LF loop and the associated impedance and diffusion parameters. As expected, the LF loop increases along the air flow field, i.e. with the segment number, but is less uniform for serpentine flow fields than for linear gas channels (Figure 5). This confirms that measuring artefacts significantly influence the LF loop of EI spectra [30–32,47], especially of those measured near the oxygen outlet and the global spectrum. A possibility to minimize their impact on EI analyses could be to focus on local spectra measured near the air inlet.

Table 13. Characteristic diffusion parameters identified from the local spectra measured on the first 5 segments of cell C using a MEA with cathode Pt loading of 0.05 mg_{Pt} cm^{-2} (Figure 8) with the EECs of Figure 2a (Warburg CCL) and b (Kulikovsky GDL).

Segment \ Model		Warburg CCL – ionomer A_{Pt}	Warburg CCL – pores A_{geom}	Kulikovsky GDL
Segment 1	**δ [µm]**	143	195	186
	D_{eff} [m² s^{-1}] 10^{-6}	0.52	0.97	0.91
Segment 2	**δ [µm]**	123	172	163
	D_{eff} [m² s^{-1}] 10^{-6}	0.42	0.82	0.77
Segment 4	**δ [µm]**	112	163	158
	D_{eff} [m² s^{-1}] 10^{-6}	0.34	0.73	0.70
Segment 5	**δ [µm]**	143	193	184
	D_{eff} [m² s^{-1}] 10^{-6}	0.59	1.08	1.01

Table 13 shows the characteristic diffusion length δ and the effective diffusion coefficient D_{eff} determined for the first five segments of cell C obtained by fitting the local EI spectra in Figure 8 (cathode Pt loading: 0.05 mg_{Pt} cm^{-2}) with the EECs of Figure 2a (Warburg CCL) and b (Kulikovsky GDL). As before, the estimation is made using a macroscopic approach (with respect to the MEA flat surface A_{geom}) for the Warburg CCL and Kulikovsky GDL configuration which allows to refer to oxygen diffusion through the pores of these layers. The microscopic point of view (with respect to the active Pt area $A_{\mathrm{Pt}} = \gamma A_{\mathrm{geom}}$) is only applied for Z_{W} in CCL-ionomer configuration as it refers to diffusion through the ionomer film in the CCL pores.

The same observation as for the global spectrum in Figure 7d) is made for the local spectra of all segments, including the first one which should be less subjected to concentration oscillations: the values obtained for δ are of the order of a GDL thickness, even if slightly

lower than those obtained for MEA with higher Pt loadings. The values of D_{eff} are of the order of oxygen diffusion in vapor phase through the GDL when adopting the macroscopic approach and thought the CCL pores when using the microscopic approach (Table 6). The evolution of δ and D_{eff} with increasing segment number is consistent with that of the LF loop of the spectra as stated above, supporting the hypothesis of a considerable contribution of measuring artefacts. No further comment is therefore done on this aspect.

The analysis of the local impedance data measured with cell C for a MEA with a cathode Pt loading of 0.05 mg_{Pt} cm^{-2} confirms the conclusions drawn from the global impedance spectrum and on the other cells regarding the layer being at the main origin of oxygen diffusion impedance: the main contribution seems to originate from the GDL, or both the GDL *and* the CCL pores. The contribution of the latter is lower than that of the GDL. The impact of the ionomer film seems negligible. This layer rather contributes to the high frequency resistance, whose impact increases when lowering the catalyst loading. Based on these observations, the most appropriate EEC for interpreting the impedance spectra measured with cell C would thus again be a modified Randles EEC with a Kulikovsky diffusion impedance connected in series with the ORR circuit (Figure 2b).

5. Conclusions

The position and expression of the diffusion impedance in PEMFC equivalent electrical circuits (EECs) is discussed to identify the layer at its origin. For this, two EEC configurations are compared:

- a series connection with the charge transfer resistance inside the ORR circuit (classical Randles model) which implies that the CCL is limiting for oxygen diffusion;
- a series connection with the ORR circuit when supposing the GDL limiting (modified Randles circuit – GDL configuration).

An EEC with both diffusion impedances, one inside the CCL circuit and one connected in series, was also tested. It turned out that one of both diffusion impedances becomes

negligible when trying to identify the impedance parameters from experimental data. That is why only EECs with one diffusion impedance are used for fitting experimental EIS spectra.

Concerning the oxygen diffusion impedance expression, the results obtained using a classical finite Warburg impedance are compared to those obtained with an alternative expression derived by Kulikovsky for the GDL. This expression accounts for the impact of ORR kinetics to oxygen diffusion.

The analysis is made on both, simulated spectra starting from theoretical characteristic values of each layer taken from the literature, and experimental data coming from 8 different configurations (MEA/geometry/operating conditions). Theoretical and experimental results lead to identical conclusions regarding the oxygen diffusion impedance, summarized as follows.

Concerning fit quality and the values of the identified impedance parameters:

- All models fit equally well the experimental data, independently of the position and the expression of the diffusion impedance in the EEC.
- Both, the location and expression of the diffusion impedance impact the estimated values of all EEC parameters, in particular those associated with oxygen diffusion and ORR kinetics. However, all configurations give comparable orders of magnitude.

To conclude about the layer associated with the LF oxygen diffusion impedance and thus the most appropriate EEC and impedance expression, the characteristic diffusion parameters, i.e. characteristic length and effective diffusion coefficient have been determined starting from the impedance parameters. For all tested EEC configurations and analyzed devices (cells and MEAs):

- values of the diffusion length are of the order of a GDL thickness;
- the effective diffusion coefficient is of the order of oxygen diffusion in air through a GDL.

These observations are independent from the surface considered, i.e. MEA flat surface (macroscopic approach) or active area $A_{\mathrm{Pt}} = \gamma A_{\mathrm{geom}}$ (microscopic approach). This leads to the conclusion that the cathode gas diffusion layer should be the main contributor to the oxygen diffusion impedance in the LF domain of PEMFC impedance spectra. The cathode catalyst layer might contribute, but to a much lower extent. Analyses of theoretical impedance spectra completed by those measured on MEAs with different Pt loadings at the cathode indicate that the ionomer film might play a role in oxygen transport limitations, but rather through a contribution to the high frequency resistance, which is impossible to decorrelate from the other cell resistances from the time being. The physically most appropriate EEC would thus be a modified Randles EEC in GDL configuration, *i.e.* a Kulikovsky diffusion impedance connected in series with the ORR kinetics circuit.

Finally, the comparison of global and local impedance spectra and their interpretation confirmed the significant contribution of measuring signal induced oxygen concentration oscillations to the low frequency loop in the Nyquist plot. Their influence increases along the air flow fields and impacts thus as well the global spectrum. Our results indicate that analyzing local impedance data measured near the oxygen inlet allows to minimize their impact. Nonetheless, the conclusions about the layer contributing most tor oxygen diffusion impedance and thus the most appropriate EEC is independent of these artefacts.

Acknowledgments

This work has received funding from the European Union's EIT Raw Materials project nº 19247, ALPE: "Advanced Low-Platinum hierarchical Electrocatalysts for low-T fuel cells, as well as from the region Grand Est, the European Fund for Economic and Regional Development FEDER, the French Environmental and Energy Management Agency ADEME and the French National Research Agency ANR - projects LOCALI and MULTISTABLE (ANR-17-CE05-0016 and ANR-18-CE05-0027).

References

[1] I. Pivac, F. Barbir, Inductive phenomena at low frequencies in impedance spectra of proton exchange membrane fuel cells – A review, J. Power Sources. 326 (2016) 112–119. https://doi.org/10.1016/j.jpowsour.2016.06.119.

[2] P.M. Gomadam, J.W. Weidner, Analysis of electrochemical impedance spectroscopy in proton exchange membrane fuel cells, Int. J. Energy Res. 29 (2005) 1133–1151. https://doi.org/10.1002/er.1144.

[3] P. Millet, N. Mbemba, S.A. Grigoriev, V.N. Fateev, A. Aukauloo, C. Etiévant, Electrochemical performances of PEM water electrolysis cells and perspectives, Int. J. Hydrogen Energy. 36 (2011) 4134–4142. https://doi.org/10.1016/j.ijhydene.2010.06.105.

[4] S.H. Frensch, A.C. Olesen, S.S. Araya, S.K. Kær, Model-supported characterization of a PEM water electrolysis cell for the effect of compression, Electrochim. Acta. 263 (2018) 228–236. https://doi.org/10.1016/j.electacta.2018.01.040.

[5] S. Siracusano, S. Trocino, N. Briguglio, V. Baglio, A. Aricò, Electrochemical Impedance Spectroscopy as a Diagnostic Tool in Polymer Electrolyte Membrane Electrolysis, Materials (Basel). 11 (2018) 1368. https://doi.org/10.3390/ma11081368.

[6] D.I. Abouelamaiem, G. He, T.P. Neville, D. Patel, S. Ji, R. Wang, I.P. Parkin, A.B. Jorge, M.-M. Titirici, P.R. Shearing, D.J.L. Brett, Correlating electrochemical impedance with hierarchical structure for porous carbon-based supercapacitors using a truncated transmission line model, Electrochim. Acta. 284 (2018) 597–608. https://doi.org/10.1016/j.electacta.2018.07.190.

[7] P.L. Taberna, P. Simon, J.F. Fauvarque, Electrochemical Characteristics and Impedance Spectroscopy Studies of Carbon-Carbon Supercapacitors, J. Electrochem. Soc. 150 (2003) A292. https://doi.org/10.1149/1.1543948.

[8] L.M. Da Silva, R. Cesar, C.M.R. Moreira, J.H.M. Santos, L.G. De Souza, B.M. Pires, R. Vicentini, W. Nunes, H. Zanin, Reviewing the fundamentals of supercapacitors and the difficulties involving the analysis of the electrochemical findings obtained for porous electrode materials, Energy Storage Mater. 27 (2020) 555–590. https://doi.org/10.1016/j.ensm.2019.12.015.

[9] U. Tröltzsch, O. Kanoun, H.-R. Tränkler, Characterizing aging effects of lithium ion batteries by impedance spectroscopy, Electrochim. Acta. 51 (2006) 1664–1672. https://doi.org/10.1016/j.electacta.2005.02.148.

[10] D. Andre, M. Meiler, K. Steiner, C. Wimmer, T. Soczka-Guth, D.U. Sauer, Characterization of high-power lithium-ion batteries by electrochemical impedance spectroscopy. I. Experimental investigation, J. Power Sources. 196 (2011) 5334–5341. https://doi.org/10.1016/j.jpowsour.2010.12.102.

[11] C.. Chen, J. Liu, K. Amine, Symmetric cell approach and impedance spectroscopy of high power lithium-ion batteries, J. Power Sources. 96 (2001) 321–328. https://doi.org/10.1016/S0378-7753(00)00666-2.

[12] B. Pejcic, R. De Marco, Impedance spectroscopy: Over 35 years of electrochemical sensor optimization, Electrochim. Acta. 51 (2006) 6217–6229. https://doi.org/10.1016/j.electacta.2006.04.025.

[13] S. Touhami, J. Mainka, J. Dillet, S.A.H. Taleb, O. Lottin, Transmission Line Impedance Models Considering Oxygen Transport Limitations in Polymer Electrolyte Membrane Fuel Cells, J. Electrochem. Soc. 166 (2019) F1209–F1217. https://doi.org/10.1149/2.0891915jes.

[14] J. Zhang, Y. Tang, C. Song, X. Cheng, J. Zhang, H. Wang, PEM fuel cells operated at 0% relative humidity in the temperature range of 23–120°C, Electrochim. Acta. 52 (2007) 5095–5101. https://doi.org/10.1016/j.electacta.2007.02.002.

[15] W. Mérida, D.A. Harrington, J.M. Le Canut, G. McLean, Characterisation of proton

exchange membrane fuel cell (PEMFC) failures via electrochemical impedance spectroscopy, J. Power Sources. 161 (2006) 264–274. https://doi.org/10.1016/j.jpowsour.2006.03.067.

[16] J.-M. Le Canut, R.M. Abouatallah, D.A. Harrington, Detection of Membrane Drying, Fuel Cell Flooding, and Anode Catalyst Poisoning on PEMFC Stacks by Electrochemical Impedance Spectroscopy, J. Electrochem. Soc. 153 (2006) A857. https://doi.org/10.1149/1.2179200.

[17] J.W. Lim, Y.-H. Cho, M. Ahn, D.Y. Chung, Y.-H. Cho, N. Jung, Y.S. Kang, O.-H. Kim, M.J. Lee, M. Kim, Y.-E. Sung, Ionic Resistance of a Cathode Catalyst Layer with Various Thicknesses by Electrochemical Impedance Spectroscopy for PEMFC, J. Electrochem. Soc. 159 (2012) B378–B384. https://doi.org/10.1149/2.030204jes.

[18] F. Ciucci, Modeling electrochemical impedance spectroscopy, Curr. Opin. Electrochem. 13 (2019) 132–139. https://doi.org/10.1016/j.coelec.2018.12.003.

[19] A. Nenning, A.K. Opitz, T.M. Huber, J. Fleig, A novel approach for analyzing electrochemical properties of mixed conducting solid oxide fuel cell anode materials by impedance spectroscopy, Phys. Chem. Chem. Phys. 16 (2014) 22321–22336. https://doi.org/10.1039/C4CP02467B.

[20] E. Ivers-Tiffée, A. Weber, Evaluation of electrochemical impedance spectra by the distribution of relaxation times, J. Ceram. Soc. Japan. 125 (2017) 193–201. https://doi.org/10.2109/jcersj2.16267.

[21] K. Kobayashi, T.S. Suzuki, Distribution of Relaxation Time Analysis for Non-ideal Immittance Spectrum: Discussion and Progress, J. Phys. Soc. Japan. 87 (2018) 094002. https://doi.org/10.7566/JPSJ.87.094002.

[22] E. Quattrocchi, B. Py, A. Maradesa, Q. Meyer, C. Zhao, F. Ciucci, Deconvolution of electrochemical impedance spectroscopy data using the deep-neural-network-enhanced distribution of relaxation times, Electrochim. Acta. 439 (2023) 141499.

https://doi.org/10.1016/j.electacta.2022.141499.

[23] F. Ciucci, C. Chen, Analysis of Electrochemical Impedance Spectroscopy Data Using the Distribution of Relaxation Times: A Bayesian and Hierarchical Bayesian Approach, Electrochim. Acta. 167 (2015) 439–454. https://doi.org/10.1016/j.electacta.2015.03.123.

[24] J.E.B. Randles, Kinetics of rapid electrode reactions, Discuss. Faraday Soc. 1 (1947) 11. https://doi.org/10.1039/df9470100011.

[25] J. Ihonen, M. Mikkola, G. Lindbergh, Flooding of Gas Diffusion Backing in PEFCs, J. Electrochem. Soc. 151 (2004) A1152. https://doi.org/10.1149/1.1763138.

[26] J.P. Owejan, J.E. Owejan, W. Gu, Impact of Platinum Loading and Catalyst Layer Structure on PEMFC Performance, J. Electrochem. Soc. 160 (2013) F824–F833. https://doi.org/10.1149/2.072308jes.

[27] N. Nonoyama, S. Okazaki, A.Z. Weber, Y. Ikogi, T. Yoshida, Analysis of Oxygen-Transport Diffusion Resistance in Proton-Exchange-Membrane Fuel Cells, J. Electrochem. Soc. 158 (2011) B416. https://doi.org/10.1149/1.3546038.

[28] A. Kulikovsky, The effect of Nafion film on the cathode catalyst layer performance in a low–Pt PEM fuel cell, Electrochem. Commun. 103 (2019) 61–65. https://doi.org/10.1016/j.elecom.2019.05.003.

[29] D. Gerteisen, A. Hakenjos, J.O. Schumacher, AC impedance modelling study on porous electrodes of proton exchange membrane fuel cells using an agglomerate model, J. Power Sources. 173 (2007) 346–356. https://doi.org/10.1016/j.jpowsour.2007.04.071.

[30] I.A. Schneider, D. Kramer, A. Wokaun, G.G. Scherer, Oscillations in Gas Channels, J. Electrochem. Soc. 154 (2007) B770. https://doi.org/10.1149/1.2742291.

[31] I.A. Schneider, S.A. Freunberger, D. Kramer, A. Wokaun, G.G. Scherer, Oscillations in

Gas Channels, J. Electrochem. Soc. 154 (2007) B383. https://doi.org/10.1149/1.2435706.

[32] G. Maranzana, J. Mainka, O. Lottin, J. Dillet, A. Lamibrac, A. Thomas, S. Didierjean, A proton exchange membrane fuel cell impedance model taking into account convection along the air channel: On the bias between the low frequency limit of the impedance and the slope of the polarization curve, Electrochim. Acta. 83 (2012) 13–27. https://doi.org/10.1016/j.electacta.2012.07.065.

[33] J. Mainka, G. Maranzana, A. Thomas, J. Dillet, S. Didierjean, O. Lottin, One-dimensional Model of Oxygen Transport Impedance Accounting for Convection Perpendicular to the Electrode, Fuel Cells. 12 (2012) 848–861. https://doi.org/10.1002/fuce.201100193.

[34] E. Warburg, Ueber das Verhalten sogenannter unpolarisirbarer Elektroden gegen Wechselstrom, Ann. Der Phys. Und Chemie. 303 (1899) 493–499. https://doi.org/10.1002/andp.18993030302.

[35] A. Kulikovsky, Why impedance of the gas diffusion layer in a PEM fuel cell differs from the Warburg finite-length impedance?, Electrochem. Commun. 84 (2017) 28–31. https://doi.org/10.1016/j.elecom.2017.09.014.

[36] S. Cruz-Manzo, P. Greenwood, Study of oxygen diffusion in the cathode catalyst layer and gas diffusion layer for polymer electrolyte fuel cells with EIS, J. Electroanal. Chem. 892 (2021) 115270. https://doi.org/10.1016/j.jelechem.2021.115270.

[37] J. Mainka, G. Maranzana, J. Dillet, S. Didierjean, O. Lottin, On the estimation of high frequency parameters of Proton Exchange Membrane Fuel Cells via Electrochemical Impedance Spectroscopy, J. Power Sources. 253 (2014) 381–391. https://doi.org/10.1016/j.jpowsour.2013.12.064.

[38] S. Dierickx, T. Mundloch, A. Weber, E. Ivers-Tiffée, Advanced impedance model for double-layered solid oxide fuel cell cermet anodes, J. Power Sources. 415 (2019) 69–

82. https://doi.org/10.1016/j.jpowsour.2019.01.043.

[39] S. Touhami, L. Dubau, J. Mainka, J. Dillet, M. Chatenet, O. Lottin, Anode aging in polymer electrolyte membrane fuel Cells I: Anode monitoring by ElectroChemical impedance spectroscopy, J. Power Sources. 481 (2021) 228908. https://doi.org/10.1016/j.jpowsour.2020.228908.

[40] S. Touhami, M. Crouillere, J. Mainka, J. Dillet, C. Nayoze-Coynel, C. Bas, L. Dubau, A. El Kaddouri, F. Dubelley, F. Micoud, M. Chatenet, Y. Bultel, O. Lottin, Anode defects' propagation in polymer electrolyte membrane fuel cells, J. Power Sources. 520 (2022) 230880. https://doi.org/10.1016/j.jpowsour.2021.230880.

[41] G. De Moor, C. Bas, N. Charvin, J. Dillet, G. Maranzana, O. Lottin, N. Caqué, E. Rossinot, L. Flandin, Perfluorosulfonic acid membrane degradation in the hydrogen inlet region: A macroscopic approach, Int. J. Hydrogen Energy. 41 (2016) 483–496. https://doi.org/10.1016/j.ijhydene.2015.10.066.

[42] R. Riasse, C. Lafforgue, F. Vandenberghe, F. Micoud, A. Morin, M. Arenz, J. Durst, M. Chatenet, Benchmarking proton exchange membrane fuel cell cathode catalyst at high current density: A comparison between the rotating disk electrode, the gas diffusion electrode and differential cell, J. Power Sources. 556 (2023) 232491. https://doi.org/10.1016/j.jpowsour.2022.232491.

[43] R. Sgarbi De Moraes, W. Ait Idir, Q. Labarde, M. Mermoux, P. Wu, J. Mainka, J. Dillet, C. Marty, F. Micoud, O. Lottin, M. Chatenet, Does the platinum-loading in proton-exchange membrane fuel cell cathodes influence the durability of the membrane-electrode assembly?, Ind. Chem. Mater. (2023). https://doi.org/10.1039/D3IM00059A.

[44] R. O'Hayre, D.M. Barnett, F.B. Prinz, The Triple Phase Boundary, J. Electrochem. Soc. 152 (2005) A439. https://doi.org/10.1149/1.1851054.

[45] D. Van Dao, G. Adilbish, T.D. Le, I.-H. Lee, Y.-T. Yu, Triple phase boundary and power density enhancement in PEMFCs of a Pt/C electrode with double catalyst

layers, RSC Adv. 9 (2019) 15635–15641. https://doi.org/10.1039/C9RA01741K.

[46] A.Z. Weber, A. Kusoglu, Unexplained transport resistances for low-loaded fuel-cell catalyst layers, J. Mater. Chem. A. 2 (2014) 17207–17211. https://doi.org/10.1039/C4TA02952F.

[47] J. Mainka, G. Maranzana, J. Dillet, S. Didierjean, O. Lottin, Effect of Oxygen Depletion Along the Air Channel of a PEMFC on the Warburg Diffusion Impedance, J. Electrochem. Soc. 157 (2010) B1561. https://doi.org/10.1149/1.3481560.

[48] Y. Bultel, K. Wiezell, F. Jaouen, P. Ozil, G. Lindbergh, Investigation of mass transport in gas diffusion layer at the air cathode of a PEMFC, Electrochim. Acta. 51 (2005) 474–488. https://doi.org/10.1016/j.electacta.2005.05.007.

[49] P.R. Lowe, THE COMPUTATION OF SATURATION VAPOR PRESSURE, 1974. https://apps.dtic.mil/sti/pdfs/AD0778316.pdf.

[50] R.B. Bird, Transport phenomena, Appl. Mech. Rev. 55 (2002) R1–R4. https://doi.org/10.1115/1.1424298.

[51] T.E. Springer, T.A. Zawodzinski, M.S. Wilson, S. Gottesfeld, Characterization of Polymer Electrolyte Fuel Cells Using AC Impedance Spectroscopy, J. Electrochem. Soc. 143 (1996) 587–599. https://doi.org/10.1149/1.1836485.

[52] J. Mainka, Local impedance in H2/air Proton Exchange Membrane Fuel Cells (PEMFC) Theoretical and experimental investigations, 2011.

[53] A. Fischer, J. Jindra, H. Wendt, Porosity and catalyst utilization of thin layer cathodes in air operated PEM-fuel cells, J. Appl. Electrochem. 28 (1998) 277–282. https://doi.org/10.1023/A:1003259531775.

[54] P. Gode, G. Lindbergh, G. Sundholm, In-situ measurements of gas permeability in fuel cell membranes using a cylindrical microelectrode, J. Electroanal. Chem. 518 (2002) 115–122. https://doi.org/10.1016/S0022-0728(01)00698-2.

[55] No Title, (n.d.). https://www.sglcarbon.com/en/markets-solutions/material/sigracet-fuel-cell-components/.

[56] I. V. Zenyuk, P.K. Das, A.Z. Weber, Understanding Impacts of Catalyst-Layer Thickness on Fuel-Cell Performance via Mathematical Modeling, J. Electrochem. Soc. 163 (2016) F691–F703. https://doi.org/10.1149/2.1161607jes.

[57] A. Baricci, A. Bisello, A. Serov, M. Odgaard, P. Atanassov, A. Casalegno, Analysis of the effect of catalyst layer thickness on the performance and durability of platinum group metal-free catalysts for polymer electrolyte membrane fuel cells, Sustain. Energy Fuels. 3 (2019) 3375–3386. https://doi.org/10.1039/C9SE00252A.

[58] L. Xia, M. Ni, Q. Xu, H. Xu, K. Zheng, Optimization of catalyst layer thickness for achieving high performance and low cost of high temperature proton exchange membrane fuel cell, Appl. Energy. 294 (2021) 117012. https://doi.org/10.1016/j.apenergy.2021.117012.

[59] X. Cheng, B. Yi, M. Han, J. Zhang, Y. Qiao, J. Yu, Investigation of platinum utilization and morphology in catalyst layer of polymer electrolyte fuel cells, J. Power Sources. 79 (1999) 75–81. https://doi.org/10.1016/S0378-7753(99)00046-4.

[60] T.A. Greszler, D. Caulk, P. Sinha, The Impact of Platinum Loading on Oxygen Transport Resistance, J. Electrochem. Soc. 159 (2012) F831–F840. https://doi.org/10.1149/2.061212jes.

[61] P. Schneider, M. Batool, A.O. Godoy, R. Singh, D. Gerteisen, J. Jankovic, N. Zamel, Impact of Platinum Loading and Layer Thickness on Cathode Catalyst Degradation in PEM Fuel Cells, J. Electrochem. Soc. 170 (2023) 024506. https://doi.org/10.1149/1945-7111/acb8df.

[62] P.C. Okonkwo, O.O. Ige, E.M. Barhoumi, P.C. Uzoma, W. Emori, A. Benamor, A.M. Abdullah, Platinum degradation mechanisms in proton exchange membrane fuel cell (PEMFC) system: A review, Int. J. Hydrogen Energy. 46 (2021) 15850–15865.

https://doi.org/10.1016/j.ijhydene.2021.02.078.

Author Contributions

- **William Aït Idir**: Formal analysis, Data curation, Visualization, Investigation, Writing – original draft.
- Peizhe Wu: Formal analysis, Data Curation, Investigation.
- **Ricardo Sgarbi**: Formal analysis, Data Curation, Investigation.
- **Quentin Labarde**: Formal analysis, Data Curation, Investigation.
- **Salah Touhami**: Data Curation, Investigation.
- **Meriem Daoudi**: Data Curation, Investigation.
- **Assma El kaddouri**: Conceptualization, Supervision.
- **Jean-Christophe Perrin**: Conceptualization, Supervision.
- **Jérôme Dillet**: Data Curation, Investigation.
- **Clémence Marty**: Data curation.
- **Fabrice Micoud**: Conceptualization, Writing – review & editing, Project administration, Formal analysis, Investigation.
- Marian Chatenet: Conceptualization, Writing – review & editing, Project administration, Formal analysis, Investigation.
- **Olivier Lottin**: Conceptualization, Formal analysis, Writing – review & editing, Supervision, Project administration, Investigation, Validation.
- **Julia Mainka**: Conceptualization, Formal analysis, Writing – original draft, review & editing, Visualization, Supervision, Project administration, Investigation, Validation.

Declaration of interests

☒The authors declare that they have no known competing financial interests or personal relationships that could have appeared to influence the work reported in this paper.

☐The authors declare the following financial interests/personal relationships which may be considered as potential competing interests: